JCI The Journal of Clinical Investigation

Evolutionary conservation of human ketodeoxynonulosonic acid production is independent of sialoglycan biosynthesis

Kunio Kawanishi, … , Anja Münster-Kühnel, Ajit Varki

J Clin Invest. 2021;131(5):e137681. https://doi.org/10.1172/JCI137681.

Research Article | Metabolism | Nephrology

Graphical abstract

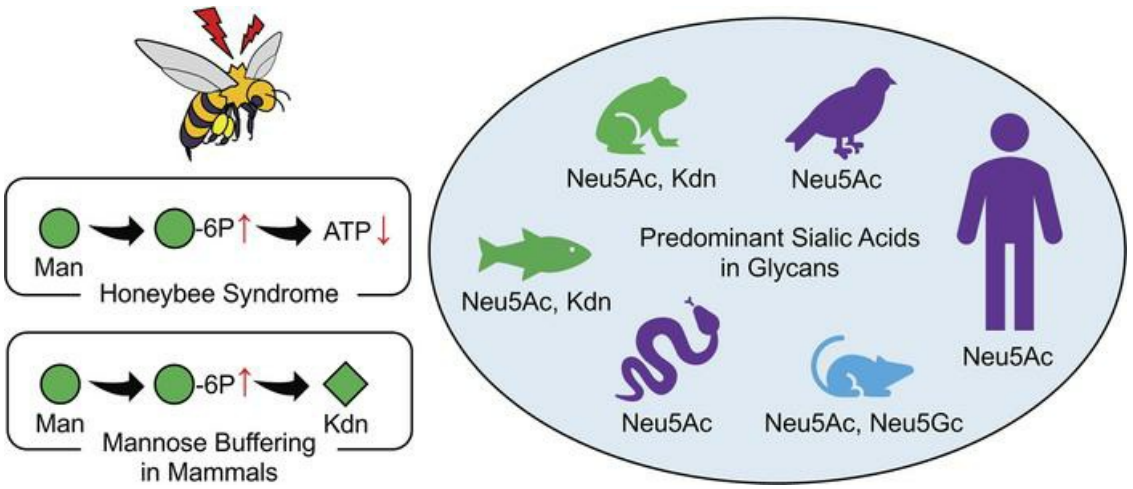

Evolutionary conservation of human ketodeoxynonulosonic acid production is independent of sialoglycan biosynthesis

Kunio Kawanishi,[1,2] Sudeshna Saha,[1,2] Sandra Diaz,[1,2] Michael Vaill,[1,2,3] Aniruddha Sasmal,[1,2] Shoib S. Siddiqui,[1,2] Biswa Choudhury,[1] Kumar Sharma,[4] Xi Chen,[5] Ian C. Schoenhofen,[6] Chihiro Sato,[7] Ken Kitajima,[7] Hudson H. Freeze,[8] Anja Münster-Kühnel,[9] and Ajit Varki[1,2,3,10]

[1]Glycobiology Research and Training Center, [2]Department of Cellular and Molecular Medicine, and [3]Center for Academic Research and Training in Anthropogeny, University of California, San Diego (UCSD), La Jolla, California, USA. [4]Center for Renal Precision Medicine, Division of Nephrology, Department of Medicine, University of Texas Health San Antonio, San Antonio, Texas, USA. [5]Department of Chemistry, University of California, Davis (UCD), Davis, California, USA. [6]Human Health Therapeutics Research Center, National Research Council of Canada, Ottawa, Ontario, Canada. [7]Bioscience and Biotechnology Center, Nagoya University, Nagoya, Japan. [8]Human Genetics Program, Sanford Burnham Prebys Medical Discovery Institute, La Jolla, California, USA. [9]Clinical Biochemistry, Hannover Medical School, Hannover, Germany. [10]Department of Medicine, UCSD, La Jolla, California, USA.

Human metabolic incorporation of nonhuman sialic acid (Sia) *N*-glycolylneuraminic acid into endogenous glycans generates inflammation via preexisting antibodies, which likely contributes to red meat–induced atherosclerosis acceleration. Exploring whether this mechanism affects atherosclerosis in end-stage renal disease (ESRD), we instead found serum accumulation of 2-keto-3-deoxy-D-glycero-D-galacto-2-nonulosonic acid (Kdn), a Sia prominently expressed in cold-blooded vertebrates. In patients with ESRD, levels of the Kdn precursor mannose also increased, but within a normal range. Mannose ingestion by healthy volunteers raised the levels of urinary mannose and Kdn. Kdn production pathways remained conserved in mammals but were diminished by an M42T substitution in a key biosynthetic enzyme, *N*-acetylneuraminate synthase. Remarkably, reversion to the ancestral methionine then occurred independently in 2 lineages, including humans. However, mammalian glycan databases contain no Kdn-glycans. We hypothesize that the potential toxicity of excess mannose in mammals is partly buffered by conversion to free Kdn. Thus, mammals probably conserve Kdn biosynthesis and modulate it in a lineage-specific manner, not for glycosylation, but to control physiological mannose intermediates and metabolites. However, human cells can be forced to express Kdn-glycans via genetic mutations enhancing Kdn utilization, or by transfection with fish enzymes producing cytidine monophosphate–Kdn (CMP-Kdn). Antibodies against Kdn-glycans occur in pooled human immunoglobulins. Pathological conditions that elevate Kdn levels could therefore result in antibody-mediated inflammatory pathologies.

Introduction

Sialic acids (Sias) are a diverse family of 9-carbon backbone monosaccharides found in glycosidic linkage to outer tips of the glycan forest that covers all vertebrate cells and most secreted macromolecules (1–5). Given their widespread expression and localization, Sias have diverse roles in biology, evolution, and disease (2, 6–10). The 2 most common mammalian Sias are *N*-acetylneuraminic acid (Neu5Ac) and *N*-glycolylneuraminic acid (Neu5Gc). Neu5Gc is hydroxylated from Neu5Ac by cytidine monophosphate-*N*-acetylneuraminic acid hydroxylase (CMAH). Humans cannot synthesize Neu5Gc because of inactivation of the *CMAH* gene that occurred about 2–3 million years ago (11). We previously reported that most humans have circulating polyclonal antibodies against glycans bearing Neu5Gc (12, 13) and that anti–Neu5Gc-glycan antibody generation correlates with the introduction of Neu5Gc during weaning (14). When exogenous Neu5Gc of dietary origin gets metabolically incorporated into sites such as epithelium and endothelium (15), glycans bearing this Sia act as foreign "xeno-autoantigens," triggering inflammatory responses termed "xenosialitis" (13, 16–19). Disease-escalating effects of xenosialitis have been demonstrated in cancer and atherosclerosis models using human-like *Cmah*-null mice (20, 21).

2-Keto-3-deoxy-D-glycero-D-galacto-nonulosonic acid (Kdn) is another vertebrate Sia that was first discovered in the cortical alveolar polysialoglycoprotein of rainbow trout eggs (22) and is abundant in cold-blooded vertebrates. Although glycosidically conjugated Kdn was not originally found in mammals (23), free Kdn was detected in porcine submaxillary glands (23), cow milk products, human urine (24), and porcine milk (25). Elevated levels of free Kdn (and indirect evidence suggesting very low levels of conjugated Kdn) have also been reported in human ovarian (26) and throat cancers (27), and free cytosolic Kdn–containing *N*-glycans accumulate in human prostate cancers (28). Monoclonal anti-Kdn antibodies produced from Kdn-immunized mice also detected very small amounts of Kdn in rat pancreas (29, 30). Another

Authorship note: K. Kawanishi and SS contributed equally to this work.
Conflict of interest: The authors have declared that no conflict of interest exists.

Submitted: March 2, 2020; **Accepted:** December 22, 2020; **Published:** March 1, 2021.
Reference information: *J Clin Invest*. 2021;131(5):e137681.
https://doi.org/10.1172/JCI137681.

monoclonal antibody against poly (2-8–linked) Kdn indicated the presence of this structure on megalin in the kidney (31–33), on cells of certain types of cancer (33), as well as on ceruloplasmin (34). However, to our knowledge, conclusive evidence for the occurrence of Kdn-glycans in normal human tissues is still missing.

Free Kdn is synthesized in the cytosol (refs. 35, 36 and Figure 1) from mannose 6-phosphate (Man-6P) (a C-2 epimer of glucose 6-phosphate) — which is itself used for the biosynthesis of *N*-linked glycans found on most secretory proteins — as a core component of glycosylphosphatidylinositol (GPI) anchors and as a metabolic precursor of fucose (37). Importantly, unlike many other free monosaccharides, mannose is very efficiently taken up by different cell types using a transporter that is insensitive to glucose (38, 39). Although specific mannose transporters have not been identified yet, mannose uptake suggests that endogenous mannose production may sometimes be inadequate for cellular requirements and that salvaging extracellular free mannose can be important.

Oral mannose administration can directly contribute to *N*-glycan synthesis (40), however, Man-6P is also endogenously derived from fructose-6-phosphate (Fru-6P) through phosphomannose isomerase (PMI) (ref. 39 and Figure 1). Inherited deficiency of PMI results in congenital disorder of glycosylation, type Ib (CDG-Ib) (PMI-CDG) associated with protein loss in intestines, liver disease, hypoglycemia, and blood-clotting disorders (41), and these patients respond well to oral mannose therapy (42). On the other hand, excessive mannose is toxic for honeybees (43, 44) and can blind baby PMI-KO mice (45). In both instances, there is a low ratio of PMI relative to hexokinase. This imbalance produces a metabolic flux, in which mannose is rapidly phosphorylated, but Man-6P cannot be efficiently converted to glycolytic intermediates. Thus, adenosine triphosphate (ATP) is wasted to produce a molecule without metabolic value to the cell, an effect that has been termed the "honeybee syndrome" (44, 46).

Although oral mannose is a potential therapeutic nutraceutical to treat certain types of CDG type I disorders (47), mannose supplements are also used to suppress urinary tract infections by *Escherichia coli* that bind mannose-rich glycans (48–50). Furthermore, recent murine studies showed that mannose supplementation has an immunosuppressive effect by inducing Tregs (51) and ameliorating high-fat diet–induced obesity and glucose tolerance by changing the microbiome profile (52). Several human studies revealed the association between increased plasma mannose levels and the risk of diabetes (53, 54), cardiovascular disease (55), and colorectal cancer risk (56). A recent study also suggested that mannose administration impairs tumor growth and enhances chemotherapy (57). However, to date, no comprehensive study has been performed to understand potential mannose toxicity in humans or the possibility of the regulation of physiological mannose homeostasis via conversion to Kdn.

Here, we report that, although serum-free mannose levels were increased but still maintained in an almost-normal range in patients with end-stage renal disease (ESRD) receiving hemodialysis, their free serum Kdn levels were substantially elevated. Furthermore, we show that humans not only excrete excess mannose into urine, but also metabolize it into free Kdn and excrete the Sia into urine, presumably to modulate mannose levels.

We also assess the evolutionary conservation (and/or convergent evolution) of genes encoding Kdn metabolic enzymes and hypothesize that the conservation of Kdn biosynthesis helps to detoxify excess Man-6P and Fru-6P. We also show that mannose-fed mammalian cells produced free Kdn in their cytosol, with predicted increases in certain genetic mutants, and that humans can have antibodies against glycosidically linked Kdn glycoconjugates (hereafter called Kdn-glycans).

Results

Increased circulating free Kdn in patients with ESRD. Previous studies in human-like *Cmah*-null mice showed that orally ingested glycosidically conjugated Neu5Gc can be metabolically incorporated into tissues, most prominently into epithelial and endothelial cells, driving antibody- and complement-mediated inflammatory progression of carcinomas (20) and atherosclerosis (21). In contrast, ingested free Neu5Gc is excreted rapidly into the urine of both rodents (58, 59) and humans (15). On the other hand, sustained, high-level exposure of cultured human cells to free Neu5Gc can result in incorporation that is sufficient to generate human anti–Neu5Gc-glycan antibody–mediated and complement-mediated inflammation (60). Thus, we hypothesized that accumulation of free Neu5Gc from the diet contributes to accelerated atherosclerosis in patients with ESRD. To explore this hypothesis, we examined free Sia profiles in sera collected from anonymized hemodialysis patients just prior to their weekly dialysis and compared them with samples from healthy volunteers. We did not see free Neu5Gc peaks in either ESRD or control sera, but instead observed a significant accumulation of other DMB-reactive α-ketoacids including Kdn and Neu5Ac in the ESRD samples (Figure 2, A–D, and Supplemental Figure 1; supplemental material available online with this article; https://doi.org/10.1172/JCI137681DS1). We confirmed the identity of Kdn and Neu5Ac peaks by liquid chromatography–mass spectrometry (LC-MS) (Supplemental Figure 2) using commercially available standards (Supplemental Table 1). Interestingly, we also noted a slight increase in 3-deoxy-D-manno-oct-2-ulosonic acid (Kdo), a bacterial octulosonic acid and component of plant polysaccharides, and other unknown peaks only in ESRD samples (Supplemental Figure 2). Serum-free Kdn levels in patients with ESRD were significantly elevated compared with levels in healthy volunteers (2.91 [0.68] μM vs. 0.50 [0.25] μM, mean [SD], $P < 0.001$; Figure 2B), as were the levels of serum-free Neu5Ac (16.9 [2.01] μM vs. 2.34 [0.54] μM, $P < 0.001$; Figure 2C). Although the levels of mannose (the metabolic precursor of Kdn) in patients with ESRD were significantly higher than those in healthy volunteers (83.8 [15.1] μM vs. 44.5 [19.1] μM, $P < 0.001$; Figure 2D), the levels in most patients with ESRD (10 of 16 patients) were within the normal range for humans (40–80 μM) (61).

Ingested mannose is partially converted to Kdn and excreted into urine in humans. We next asked whether feeding mannose to healthy humans would result in increased Kdn production. In prior studies involving healthy humans, feeding mannose at 0.10–0.25 g/kg body weight resulted in a peak concentration of mannose in the blood of approximately 0.5 mM, with only mild gastrointestinal symptoms in 1 individual. However, at oral doses exceeding 0.25 g mannose/kg body weight, approximately half of the subjects reported mild gastrointestinal distress. No other symptoms were reported (47). We therefore studied healthy humans during

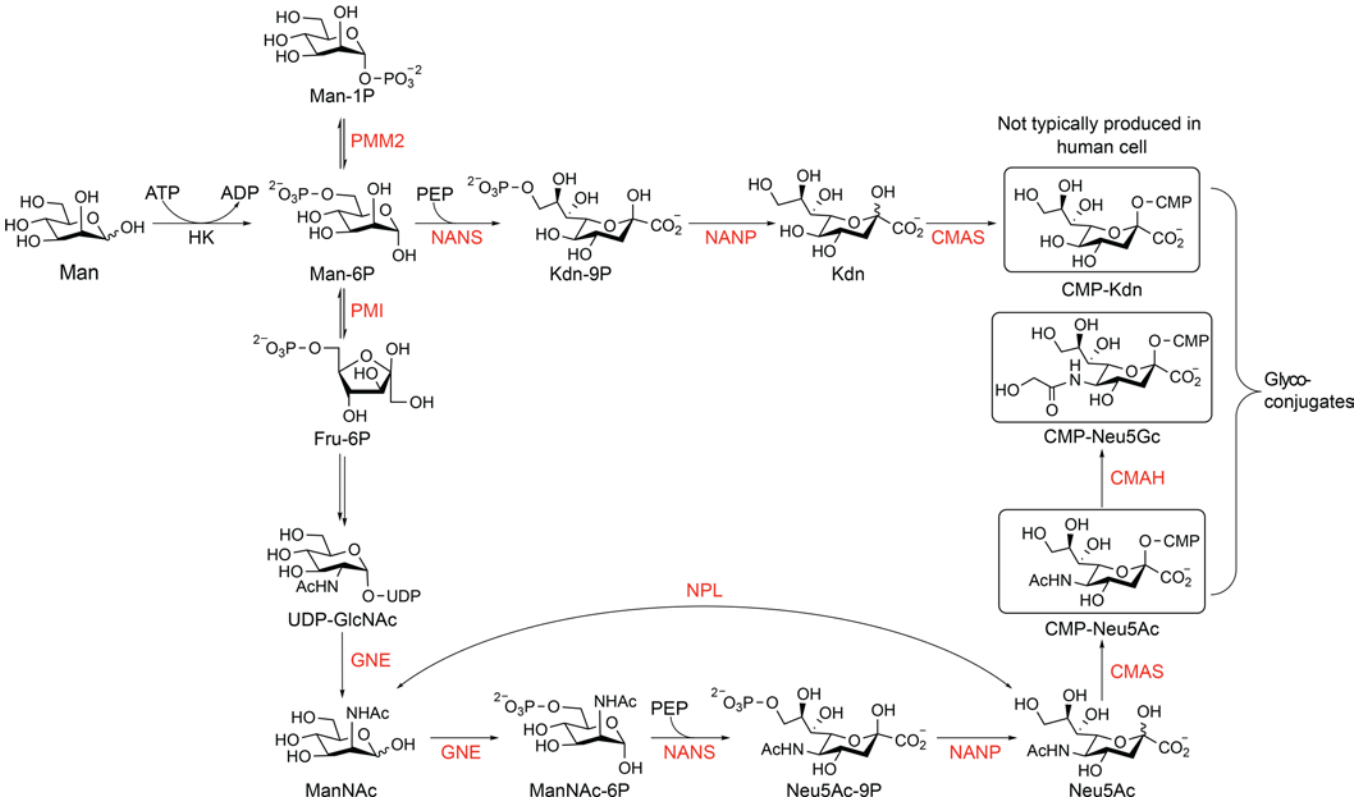

Figure 1. Metabolic pathway associated with mannose and Sias. Mannose is associated with Sia metabolism. Mannose is phosphorylated to Man-6P by hexokinase and ATP as a cofactor. Man-6P is converted to Kdn with NANS and *N*-acetylneuraminic acid phosphatase (NANP), and Kdn can be converted to CMP-Kdn with CMP *N*-acetylneuraminic acid synthetase (CMAS) in some species. Man-6P can also be transformed into Man-1P by phosphomannomutase 2 (PMM2). Man-6P is also converted to Fru-6P by PMI. Fru-6P is transformed into uridine diphosphate *N*-acetylglucosamine (UDP-GlcNAc), which is then converted to ManNAc-6P via GNE. ManNAc-6P is converted to Neu5Ac via NANS and NANP. NPL regulates Neu5Ac concentrations by mediating the reversible conversion to ManNAc and pyruvate, but human NPL does not work on Kdn. Neu5Ac is converted to CMP-Neu5Ac with CMAS, and CMP-Neu5Ac is converted to CMP-*N*-glycolylneuraminic acid (Neu5Gc) by CMAH. Humans cannot synthesize Neu5Gc because of inactivation of the *CMAH* gene about 2–3 million years ago.

mannose ingestion at 0.20 g/kg body weight. No obvious symptoms were reported, and serum mannose levels, measured by gas chromatography–mass spectrometry (GC-MS), rose 1 hour after ingestion to a maximum of 285 μM (mean) and decreased subsequently within 8 hours of ingestion to 120 μM (Figure 3A), as previously described (47). Urine mannose levels increased from 4 μM (mean) (before mannose ingestion) to 11 μM and then decreased to approximately 5 μM (Figure 3A). Similarly, we observed a peak of free Kdn 4 hours after ingestion that remained at this higher level (Figure 3B). Overall, following the serum mannose peak at 1 hour, both mannose and free Kdn levels in urine rose within 4 hours of ingestion (Figure 3), suggesting that excess free mannose could be directly and indirectly (metabolized to free Kdn) eliminated by urinary secretion. Serum Neu5Ac and Kdn levels did not change after oral mannose administration, consistent with a previous animal study (36) and our findings of serum Kdn elevation only in patients with ESRD and not in healthy control individuals (Figure 2). To determine whether oral mannose administration results in Man-6P accumulation in human serum and urine, we measured Man-6P concentrations after 1 hour in the serum and after 4 hours in the urine of healthy humans. We could not detect any Man-6P using high-performance anion exchange chromatography with pulsed amperometric detection (HPAEC-PAD), even after mannose ingestion (Supplemental Figure 3). One possible explanation could be that Man-6P is not exported out of the cells. Another possibility is the presence of plasma/serum phosphatases that destroy Man-6P and that those enzymes do not exist in the urine. The latter possibility is supported by the observation that exogenously added Man-6P could only be detected in urine but not in serum samples (Supplemental Figure 3, C and F). Overall, these results suggest that mannose levels may be controlled directly by the urinary system and/or indirectly by Kdn metabolic pathways.

Dose-dependent mannose toxicity in cultured human and mouse cells. To our knowledge, there is no report confirming mannose toxicity in humans. Free Kdn is synthesized in the cytosol of mammalian cells fed 20 mM mannose (35, 36). However, in vitro and in vivo studies suggest that mannose toxicity in PMI-KO cells or embryos can be caused by Man-6P accumulation, which inhibits glucose metabolism and depletes intracellular ATP (39, 40, 46). To test mannose toxicity in human cells, we performed a continuous cell viability assay for mannose-fed cultures at varying concentrations (0–200 mM), using another monosaccharide, *N*-acetylglucosamine (GlcNAc) (which is not efficiently taken up), as a control for any hyperosmolar effect (Figure 4). Human embryonic kidney 293A (HEK293A) cells and human umbilical vein endothelial cells (HUVECs) were tested as representative cells of kidney epithelium and endothelium

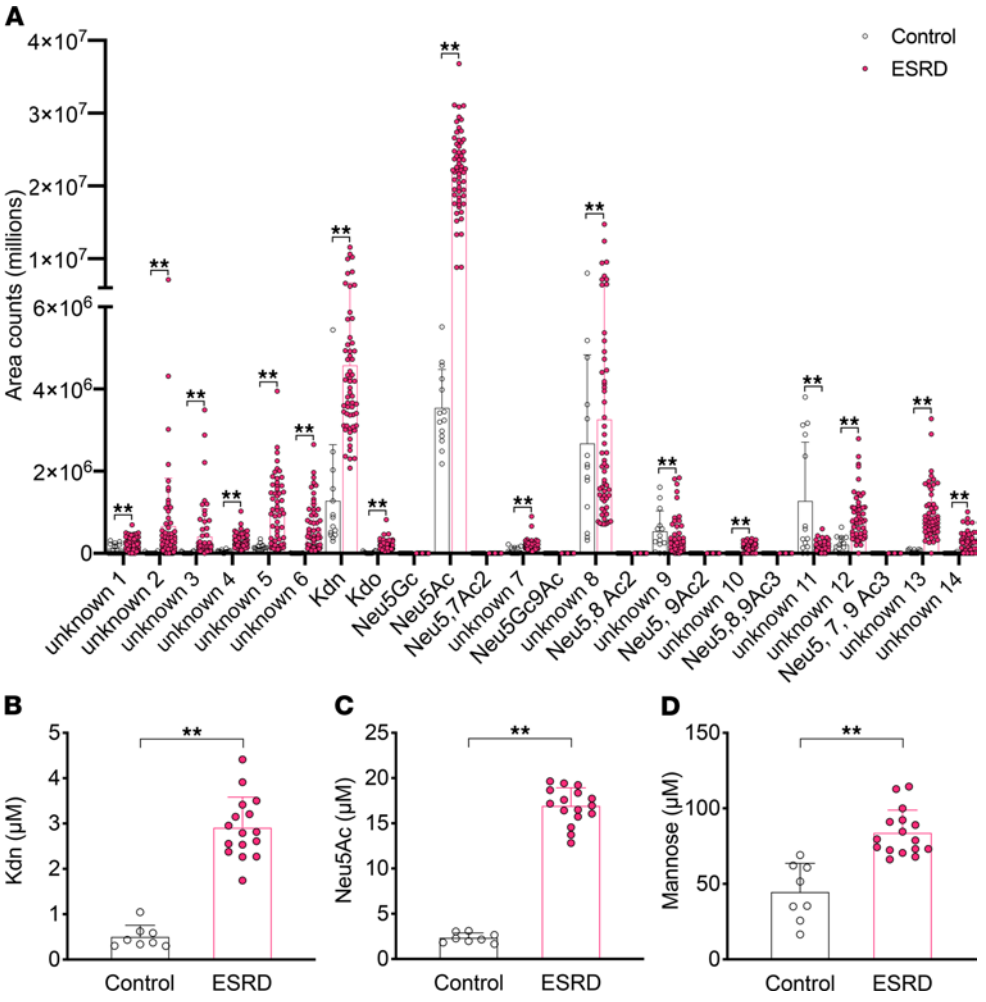

Figure 2. DMB-HPLC profiling of serum samples from patients on hemodialysis compared with serum from healthy individuals. Serum samples from (**A**) healthy volunteers (Control) (n = 14) and patients with ESRD on hemodialysis (ESRD) (n = 58) were analyzed by DMB-HPLC. Each dot represents each serum sample. Levels of the serum free (and CMP-) forms of (**B**) Kdn and (**C**) Neu5Ac were calculated with DMB-HPLC. (**D**) Serum mannose levels (normal range, 40–80 μM) were measured by GC-MS. Control (n = 8) versus ESRD (n = 16). Data are shown as the mean (SD). $^{**}P < 0.01$, by 1-way ANOVA (**A**) and unpaired t test (**B**–**D**).

encountering mannose in the blood stream, respectively. We also studied a human Burkitt's lymphoma cell line (BJAB K88, *GNE*$^{+/+}$, UDP-GlcNAc 2-epimerase/ManNAc kinase WT [GNE WT]) and a subclone deficient in Sia production (BJAB K20, *GNE*$^{-/-}$, GNE-KO) (62), as well as *PMI*$^{+/+}$ (PMI WT) and *PMI*$^{-/-}$ (PMI-KO) mouse embryonic fibroblasts (40). Neither HEK293A cells (Figure 4, A and B) nor HUVECs (Figure 4, C and D) showed differences between mannose and GlcNAc feeding, even at a high concentration (100 mM). However, the other cell lines clearly showed selective mannose toxicity at a lower concentration of 25 mM (Figure 4, E, G, and I) in comparison with GlcNAc feeding (Figure 4, F, H, and J). In particular, PMI-KO cells, when cultured at mannose concentrations higher than 1 mM (Figure 4K), displayed the "honeybee syndrome," caused by overproduction of Man-6P, as previously shown (39, 40). A previous study confirmed that PMI-KO cells had Man-6P accumulation in the physiological condition (20–100 μM mannose) and that ATP depletion started when maximum levels of Man-6P had been reached (4–8 hours of culturing with 500 μM mannose supplementation) (40). We also observed a reduction in the viability of PMI-KO cells fed GlcNAc (10–30 mM) (Figure 4L) that was caused by a yet-unknown mechanism (63) and that could have been partly associated with ATP depletion during the GlcNAc feedings. Notably, unlike all other cells tested for the effect of GlcNAc, the PMI-KO cells in Figure 4L were always maintained in media supplemented with mannose (25 μM), since this minimal mannose amount is indispensable for the viability of the PMI-KO cells.

Next, we sought to determine whether mannose feeding of the cultured cells could result in the production of cytosolic Kdn or whether the Sia upon formation is excreted into the growth media. To that end, we grew different human and mouse cells including HEK293A cells, HUVECs, BJAB K88 cells (GNE WT), and K20 cells (GNE-KO) as well as PMI WT and PMI-KO mouse embryonic fibroblasts in the presence of exogenous free mannose. On the basis of previous Kdn studies involving 20 mM mannose supplementation (35, 36) and our viability assay (Figure 4), we first tested 0, 1, 3, 5, 10, and 15 mM mannose supplementation and analyzed the concentration of Kdn relative to Neu5Ac in the cytosol (Supplemental Table 2) or in the growth media (Supplemental Table 3) by 1,2-diamino-4,5-methylenedioxybenzene–HPLC (DMB-HPLC). We decided to use 0 and 15 mM mannose supplementation conditions for all the human and PMI WT cells for further quantification (n = 3 experiments, Figure 5). Since PMI-KO cells failed to survive in the absence of mannose and required a minimal mannose concentration for their viability during the assay, we could not quantify Kdn in the mannose-depleted media for these cells. Instead, we used 25 μM (minimal concentration for cell survival), 250 μM (mimicking the maximum concentration in human sera, Figure 3A), and 1 mM mannose supplementation for Sia quantification in PMI-KO cells (n = 3 experiments, Figure 5). Analyses of purified free Sia and cytidine monophosphate (CMP-Sia) by DMB-HPLC confirmed that only CMP-Sia survived the reduction by NaBH4 (ref. 64 and Supplemental Figure 4), allowing us to distinguish between free Sia and CMP-Sia in the cytosol. Most of the cytosolic Kdn represented the free form ($NaBH_4$ sensitive; up to 1000 pmole Kdn/million cells by DMB-HPLC) (Figure 5, A–E) and not CMP-Kdn ($NaBH_4$ resistant; less than 60 pmole Kdn /million cells) (Figure 5, F–J). Unlike the other human cell lines, which showed an increase in cytosolic accumulation of Kdn, cytosolic free (and

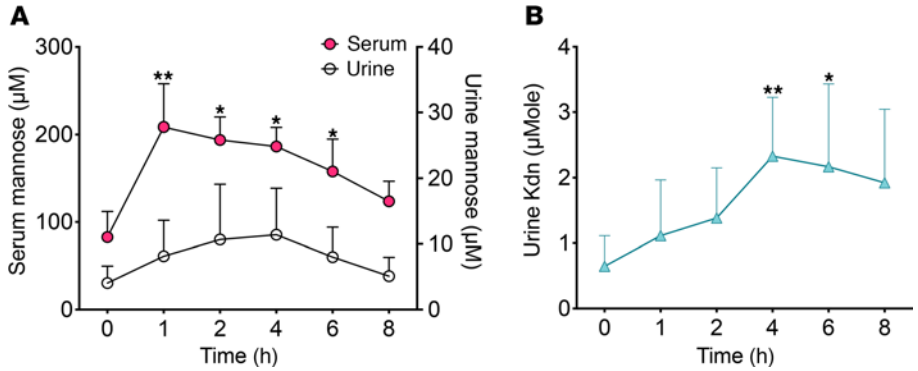

Figure 3. Human mannose ingestion test reveals increased urinary Kdn. Mannose (0.20 g/kg body weight) was used for the human ingestion test (healthy volunteers, $n = 5$). (**A**) Time course (0–8 hours after mannose ingestion) for serum and urine mannose levels, which were measured by GC-MS. (**B**) Urinary Kdn levels were evaluated by HPLC. Data are shown as the mean (SD). $^*P < 0.05$ and $^{**}P < 0.01$, by 2-way ANOVA.

CMP-) Kdn levels in HEK293A cells did not change upon mannose feeding (Figure 5A). Instead, we found that Kdn levels in the media of HEK293A cells were elevated (Supplemental Table 3). We also analyzed an immortalized proximal tubule epithelial cell line from normal adult human kidney (HK2) (65), which showed a marked elevation of Kdn in the media after mannose feeding (Supplemental Table 3). Taken together with the Sia analyses in the cytosol and media, we conclude that human and mouse cells can produce free Kdn — and secrete it from cells — by an as-yet-unknown mechanism for the possible modulation of excess Man-6P.

Glycosidically conjugated Kdn rarely occurs in mammalian glycans. For a better understanding of the Kdn sialoglycome in eukaryotes, we searched available online databases for glycans with terminal glycosidically conjugated Kdn. Although glycosidically conjugated Neu5Ac and Neu5Gc were commonly observed in different eukaryotic groups, such Kdn-glycans were only reported in fish and amphibians, and not in any mammalian cells (Table 1). Indeed, in an extensive and in-depth mass spectrometric study of *N*-glycans from murine and human cell lines and tissues conducted by the Consortium for Functional Glycomics (66) (http://www.functionalglycomics.org), there was no evidence of Kdn-glycans in the approximately 425 human and mouse cell and tissue samples studied (Anne Dell and Stuart Haslam, Imperial College London, London, United Kingdom, personal communication). Taken together, these data suggest that the capacity for utilization of Kdn as a Sia conjugated to glycans was diminished or eliminated prior to the time that vertebrates became primarily land-based.

The Kdn biosynthetic pathway is conserved throughout vertebrate phylogeny and is under purifying selection in humans. As mentioned above, there is currently no conclusive evidence of Kdn-glycans in healthy mammalian tissues. On the basis of our observation of free Kdn in urine following mannose feeding (Figure 3B), we therefore asked whether human cells contain Kdn biosynthetic enzymes required for the production of Kdn from Man-6P. We investigated 7 human genes involved in mannose metabolism and conversion of Man-6P to Kdn (Figure 1) for evolutionary conservation, comparing them with their respective homologous genes in 5 species representatives of vertebrate phylogeny (Table 2).

While previous studies identified the conservation of Sia biosynthesis pathways in mammals (67), our results demonstrate that the enzymes capable of synthesizing Kdn from Man-6P are also conserved throughout vertebrate phylogeny and are experiencing ongoing purifying selection in humans and other vertebrate species (0.005–0.347, the ratio of the nonsynonymous substitution rate [Ka] to the synonymous substitution rate [Ks], thus Ka/Ks, 64%–89% nt, and 54%–99% aa conservation) (Table 2). This finding further raises the question as to why Kdn biosynthesis is under purifying selection in organisms that do not appear to possess the capacity to utilize the monosaccharide in the synthesis of glycan structures. One explanation is that most of these genes are also involved in other conserved metabolic pathways. However, another nonmutually exclusive explanation for this selective pressure (i.e., preserving Kdn production) would be the necessity of these species to avoid the toxicity of excess Man-6P (see below).

A single aa in Sia 9-phosphate synthase that alters the rate of mannose to Kdn conversion is restored independently in 2 mammalian lineages, including humans. An earlier study showed that a single aa exchange (methionine 42 [M42] to any other aa except leucine) abolishes the ability of the human Sia 9-phosphate synthase (NANS) to synthesize Kdn-9P, while retaining its Neu5Ac-9P biosynthetic ability in vitro (68). We investigated the conservation of this key M42 position in other vertebrates. NANS protein sequences were highly conserved in a wide variety of lineages, e.g., mammalian species showed 87%–100% identity and 94%–100% homology, whereas nonmammalian vertebrates showed not less than 76% identity and 89% homology (Supplemental Table 4). We studied the phylogenetic topology including predicted ancestral aa and respective codons corresponding to M42 in human NANS (Figure 6 and Supplemental Figure 5). Considering the high homology to the human enzyme, we hypothesized that high Kdn-9P synthase activity was presumably associated with M42, also present in common ancestors. Remarkably, M42 was mainly found in nonmammalian vertebrates, e.g., aves, amphibia, and actinopterygii, in which, for the latter 2, the presence of glycosidically conjugated Kdn has been unequivocally demonstrated by MS analyses (Table 1). In mammals, M42 was found in monotremes (e.g., platypus) and metatheria (e.g., koala and opossum). In placentals, M42 was initially replaced by less active T42 but subsequently restored independently in 2 lineages: primates and artiodactyla (even-toed ungulates and cetaceans), apparently by convergent evolution. This finding again suggests an ongoing selection, possibly because of a need to modulate excess Man-6P into Kdn in clades that no longer use Kdn as a glycosidically conjugated Sia on glycoconjugates.

Mannose feeding in mutant cells can cause Kdn incorporation onto cell surfaces. Since healthy mammalian cells do not present glycosidically conjugated Kdn, we decided to include mutant cell lines in the analyses. On the basis of the cell viability assay results shown above, the highest concentration of mannose in cell

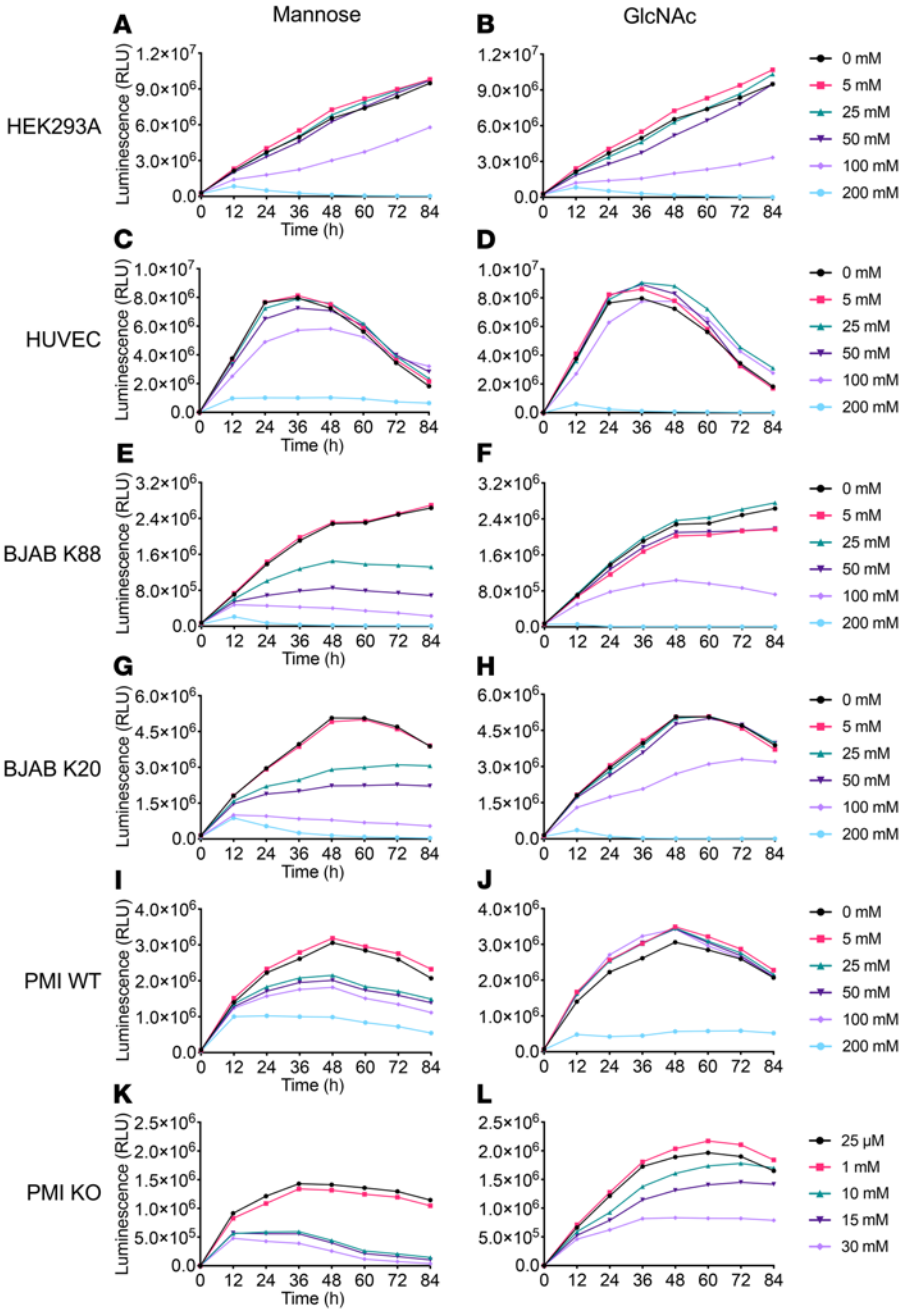

Figure 4. Toxicity of excess mannose in human and mouse cells in a dose-dependent manner. A continuous cell viability assay (0–84 hours) was performed to evaluate mannose toxicity to various human and mouse cell lines including mutants of Kdn-associated metabolic enzymes. The mannose feeding concentration was set at 0–200 mM, and the same concentration of GlcNAc was used as a control for the hyperosmolarity effect. Results shown are for (**A** and **B**) HEK293A cells; (**C** and **D**) HUVECs; (**E** and **F**) BJAB K88 cells (GNE WT); (**G** and **H**) BJAB K20 cells (GNE-KO); (**I** and **J**) PMI WT cells; and (**K** and **L**) PMI-KO cells. (**L**) PMI-KO cells were always maintained in mannose-supplemented (25 μM) media for their survival during GlcNAC feeding. Data are representative of 2 independent experiments.

culture media was determined to be 15 mM (1 mM for PMI-KO cells) to maintain optimal cell viability. As mentioned earlier, the total amount of free (and CMP-) Kdn in cytosol or media was elevated in all types of cells after mannose supplementation (Figure 5 and Supplemental Tables 2–6), but no significant increase in the concentration of CMP-Kdn (Figure 5).

To evaluate the possible production of Kdn-containing glycan structures, we analyzed the Sia content of various cell lines fed with mannose and treated with NaOH and $NaBH_4$ to destroy any unconjugated Sia, and then examined by DMB-HPLC for glycosidically conjugated Sias from the total cell lysate (Supplemental Table 4). The highest Kdn/Neu5Ac ratio was observed in BJAB K20 cells, which, because of a *GNE* mutation, cannot make internal Neu5Ac. In line with this, BJAB K20 cells also showed a high amount of free Kdn in the cytosol as well as in the media (Supplemental Tables 2 and 3). However, total conjugated Kdn levels were much lower than free and CMP-Kdn levels in the cytosol and media, even in BJAB K20 cells (Supplemental Tables 2–4). We also collected membrane fractions after ultracentrifugation, and DMB-HPLC analyses showed conjugated Kdn in the membrane fraction, especially in BJAB K20 and PMI-KO cells (Supplemental Table 5). Next, we used 2 previously reported anti–Kdn-glycan monoclonal antibodies, kdn3G (69) and kdn8kdn (70), which have specific affinities for glycans containing α2-3– or α2-8–linked Kdn, respectively, but not for α2-6-Kdn-glycan structures (29, 69). Flow cytometry using these anti-Kdn antibodies did not detect any peak shift for BJAB K20 cells (Figure 7, A and B), probably because BJAB K20 cells mainly form α2-6–linked Sia that are undetectable with the 2 antibodies used for the assay (71, 72). In contrast to BJAB K20 cells, PMI-KO cells presented small amounts of Kdn in α2-3 and α2-8 linkage on cell-surface structures upon feeding with mannose (Figure 7, C and D).

Fish Cmas gene expression plus mannose feeding can force Kdn incorporation onto some normal cell surfaces. Prior to transfer to glycans, Sias are activated into CMP-Sias, a reaction involving cytidine triphosphate (CTP) and catalyzed by CMP-Sia synthase, encoded by the CMP *N*-acetylneuraminic acid synthetase (*CMAS*) gene. As we showed earlier, Kdn incorporation into cell-surface glycans seems to be rare in comparison with free Kdn production, even after mannose feeding, probably because human CMAS and mouse CMAS preferentially work on Neu5Ac (73–75). Indeed, human CMAS has 94% identity to the murine enzyme (refs. 75, 76 and Supplemental Table 7), and the activity of the recombinant murine CMAS was 15 times lower for Kdn than for Neu5Ac (75). Our investigation into the

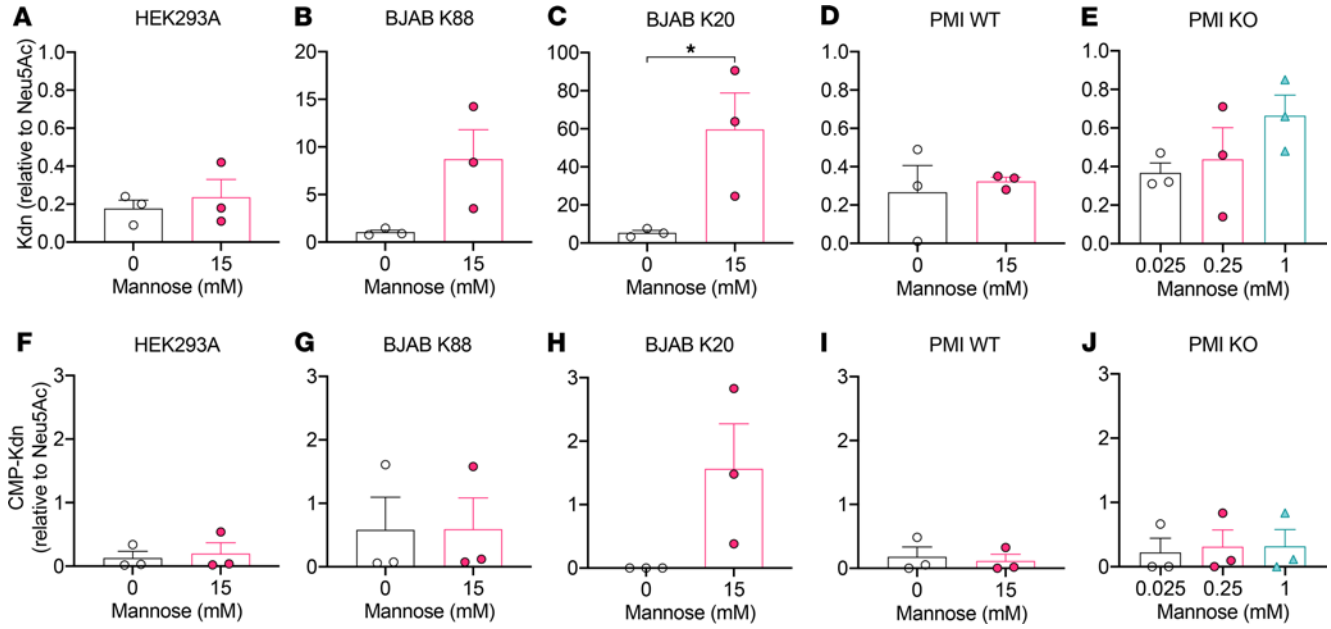

Figure 5. The Kdn/Neu5Ac ratio increases in cytosolic fractions after mannose feeding in human and mouse cell types. Levels of cytosolic free (and CMP-) Kdn (**A**–**E**) and CMP-Kdn (**F**–**J**) were measured by DMB-HPLC. Results are shown for (**A** and **F**) HEK293A cells; (**B** and **G**) BJAB K88 (GNE WT) cells; (**C** and **H**) BJAB K20 (GNE-KO) cells; (**D** and **I**) PMI WT mouse embryonic fibroblasts; and (**E** and **J**) PMI-KO cells. CMP-Sias were measured by DMB-HPLC after $NaBH_4$ treatment. The mannose concentration was set at 0 or 15 mM, except for PMI-KO cells (0.025, 0.25, and 1 mM). Data are shown as the mean (SD). *$P < 0.05$, by unpaired *t* test.

phylogenetics of these pathways brought attention to a whole-genome duplication event that occurred in the teleost lineage of fish (77). This duplication produced 2 fish *Cmas* paralogs known as *Cmas1* and *Cmas2* (78). Since our previous results showed that HEK293A cells mainly make and excrete excess free Kdn into media, recombinant zebrafish *Cmas* plasmid vectors were transfected into HEK293A cells (Figure 7E, 30%–40% of cells were transfected, by checking transfection efficiency using an anti-Flag antibody, and data not shown). Flow cytometry using anti-Kdn antibodies showed no significant peak shift in *Cmas*-transfected HEK293A cells fed with up to 15 mM mannose (data not shown). However, DMB-HPLC analysis of the membrane fraction showed that zebrafish *Cmas* transfection could result in glycosidically conjugated Kdn (exemplarily shown for *Cmas2*-transfected HEK293A cells in Figure 7, H and I). The ratio of glycosidically conjugated Kdn to Neu5Ac, especially in mannose-fed samples, was lower in *Cmas1*-transfected cells (Supplemental Table 6), consistent with differential substrate specificity in vitro (78). Interestingly, the amount of conjugated Neu5Gc (traces derived from FCS) was lower than Neu5Ac but still higher than Kdn in human cells (Figure 7, F–I), confirming a limited utility for Kdn compared with Neu5Gc in glycosylation.

Humans have circulating polyclonal antibodies against Kdn-glycans. We have previously shown that humans have varying levels of circulating antibodies against glycans bearing the nonhuman Sia Neu5Gc (13, 14, 79). Although glycosidically conjugated Kdn is not reported in normal human tissues, some malignant cells may have the potential to incorporate Kdn on their surface sialoglycans in a Kdn-rich environment. To probe for the presence of any circulating anti–Kdn-glycan antibodies, we used chemoenzymatically synthesized biotinylated glycan containing Kdn α2-3 linked to Galβ1-4GlcNAc (Figure 8A) to screen commercially available pooled normal human sera in an ELISA-based assay and found the presence of IgG antibodies against this Kdn-glycan epitope (Figure 8B). We also used Neu5Ac and Neu5Gc linked sialoglycans alongside non-sialylated glycans containing the same underlying Galβ1-4GlcNAc epitopes to determine the presence of antibodies against those corresponding epitopes (Figure 8, A and B). While our current data do not present the complete repertoire of anti–Kdn-glycan antibodies in humans, they provide evidence for the selective occurrence of such antibodies in normal human sera.

Discussion

Mannose levels in mammalian sera are variable but seem to be controlled within a restricted range (20–160 μM) (61). Levels of mannose can be affected by ingestion of mannose-rich food such as fruits, vegetables, yeasts, etc. (46, 80), by lysosomal release by *N*-glycan processing (61, 81), and by recovery and reabsorption by sodium glucose cotransporters (SGLTs) (82). SGLTs may work as mannose transporters in both intestine and kidney (82, 83). Mannose is also transported into mammalian cells via glucose transporters, but mannose-specific transporters have not yet been identified (84). Almost all transported mannose (95%–98%) is catabolized via PMI, and in [2-^{3}H]-mannose radioactive metabolic labeling experiments, only up to 2% of mannose taken up is used for *N*-glycosylation (61, 81). Interestingly, a later study using more sensitive ^{13}C-glucose and ^{2}H-mannose isotopic labeling and GC-MS analysis showed that transported mannose is utilized more efficiently than glucose: while 1.8% of transported mannose appears in *N*-glycans, only 0.026% of transported glucose is utilized in *N*-glycan synthesis (85).

Furthermore, through a nocodazole-sensitive transporter, mannose from lysosomal *N*-glycan processing is transported out of the cell as free mannose without being catabolized (81). The

Table 1. Results of glycan database searches for glycosidically linked Kdn

Database	Total number of glycan structures	Occurrence of Neu5Ac	Glycans with Neu5Ac	Glycans with Kdn	Occurrence of Kdn	Ref.
GlyGen (https://www.glygen.org)	29,290	Mammals	8963	None	(99)	
GlyConnect (https://glyconnect.expasy.org)	3435	Mammals, fish, aves, amphibians	371	35	Fish, amphibians	(100)
UniCarb-DB (https://unicarb-db.expasy.org)	1118	Mammals	415	None	(101)	
LipidBank (http://lipidbank.jp)	7009	Mammals, fish, aves, amphibians	100	17	Fish, amphibians	(102)
GlyTouCan (https://glytoucan.org)	117,832	Mammals, fish, aves, amphibians	6570	334	Fish, amphibians	(103)

Table 2. Conservation of human Kdn biosynthesis pathway genes

	PMM2	*PMI*	*NPL*	*NANS*	*NANP*	*GNE*	*CMAS*
Ka/Ks							
Homo	0.000	0.000	0.000	0.000	0.000	0.000	0.163
Mus	0.047	0.132	0.100	0.029	0.069	0.005	0.317
Gallus	0.115	0.329	0.265	0.038	0.166	0.023	0.347
Anolis	0.162	0.276	0.274	0.089	0.292	0.068	0.201
Xenopus	0.206	0.265	0.324	0.151	0.272	0.091	
Danio	0.176	0.279	0.337	0.125	0.397	0.113	[A]0.038, [B]0.264
% aa							
Homo	100	100	100	100	100	100	100
Mus	92	85	87	95	94	99	94
Gallus	85	64	71	87	72	93	77
Anolis	79	67	69	85	68	92	84
Xenopus	69	62	54	78	59	86	63
Danio	73	63	57	79	50	81	[A]60, [B]53
% nt							
Homo	100	100	100	100	100	100	100
Mus	88	87	86	89	86	88	88
Gallus	78	70	74	81	67	81	76
Anolis	75	71	71	77	72	80	78
Xenopus	67	67	64	74	74	77	68
Danio	71	69	66	74		71	[A]68, [B]75

Ka/Ks (top), percentage of aa identity (middle), and percentage of nt identity (bottom), values of genes involved in the synthesis of Sia across the vertebrate phylogeny: *Homo sapiens* (human); *Mus musculus* (mouse); *Gallus gallus* (chicken); *Anolis carolinensis* (green anole lizard), *Xenopus laevis* (African clawed frog); *Danio rerio* (zebrafish). For zebrafish: [A]*Cmas1* gene and [B]*Cmas2* gene. The whole-genome duplication event that affected *Cmas* in Teleostei also produced a paralog of *Nans*; however, the expression and function of the *Nansb* gene are unknown, so for this phylogenetic analysis, we focused on zebrafish *Nansa* (96).

reason for these separate pathways for intracellular mannose is unknown, but cells may need to eliminate excess mannose to avoid accumulation of toxic products such as Man-6P. Indeed, mannose toxicity was confirmed in our cell viability assay most prominently in PMI KO cells (Figure 4). High levels of mannose are also teratogenic in rat embryo cultures and pregnancy models, as a result of inhibition of glycolysis (86, 87).

Free Man-6P might be directly metabolized into Kdn or through the hexosamine biosynthetic pathway (Figure 1). Although human cells can synthesize Kdn from Man-6P, Kdn is not (or only in very small quantities) incorporated into glycoconjugates in healthy humans. Given all these observations, we hypothesize that Kdn synthesis is conserved in mammalian metabolism to buffer cellular levels of Man-6P. Concordantly, our phylogenetic sequence analysis suggests an underlying evolutionary pressure to conserve the metabolic pathway that converts mannose to Kdn in vertebrates (Table 2). However, the capability to incorporate Kdn into glycoconjugates differs between vertebrate classes. The apparent lack of Kdn in the glycan determinants of mammals contrasts strikingly with the previously mentioned examples of Kdn-containing structures in the gametes and mucus secretions of amphibia and fish and suggests that the enzymes necessary for Sia incorporation may have lost their

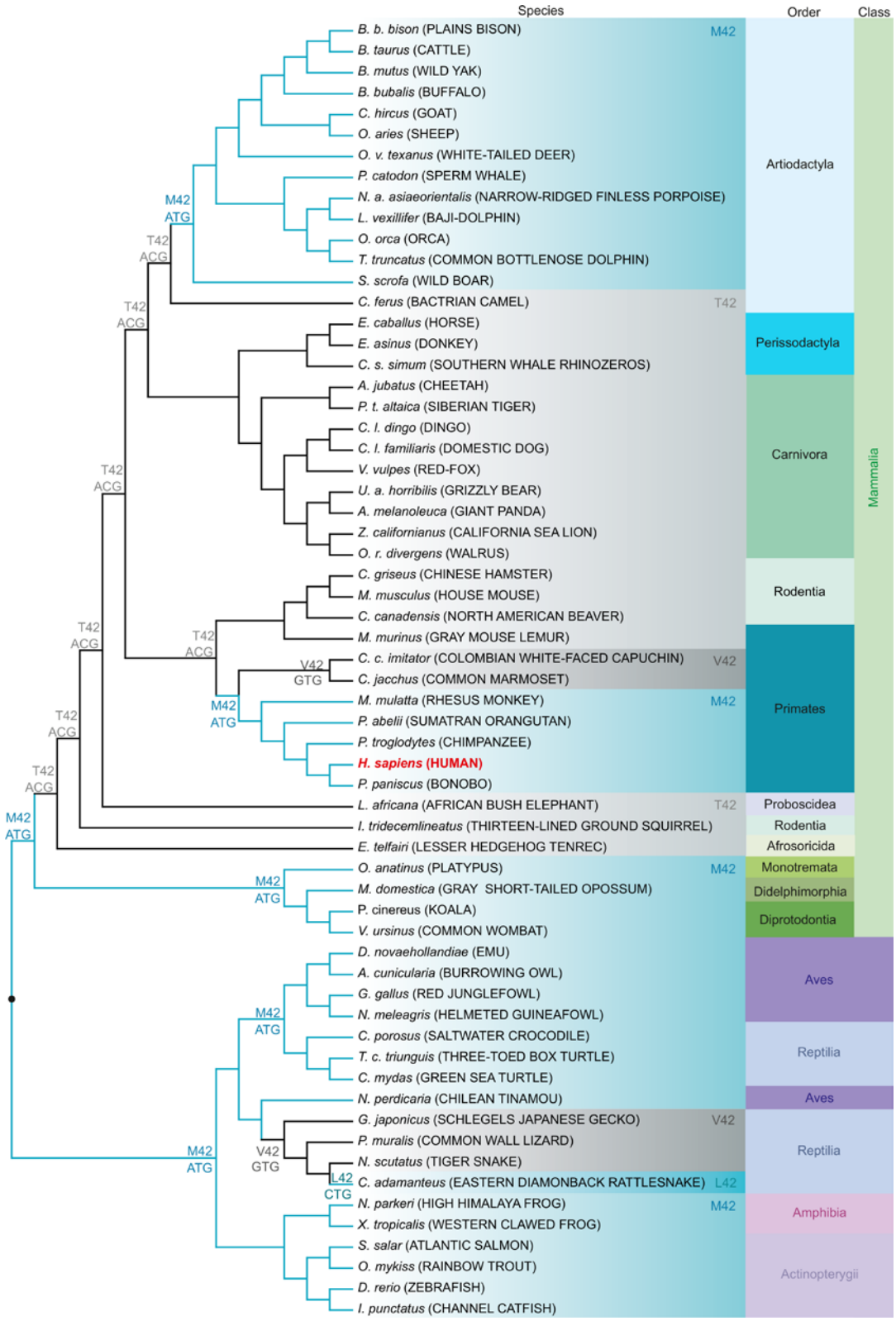

Figure 6. A single aa in Sia 9-phosphate synthase that alters the rate of mannose-to-Kdn conversion is restored independently by convergent evolution in 2 mammalian lineages including humans. Phylogenetic tree topology of vertebrate NANS nt sequences obtained using the maximum likelihood method. The tree was rooted on nonmammalian vertebrates (●) and is not drawn to scale. Human NANS with methionine or leucine at position 42 shows Kdn-9P synthase activity. Species with methionine or leucine at the position aligned to M42 in human NANS are shaded in light blue, and species with threonine (T42) or valine (V42) are shaded in light and dark gray, respectively. Predicted nt encoding the aa at the respective position in the ancestors are given at the nodes. Human NANS is shown in red. Latin species names are italicized and common names are given in uppercase letters. Mammals are further classified in orders and all vertebrates in classes.

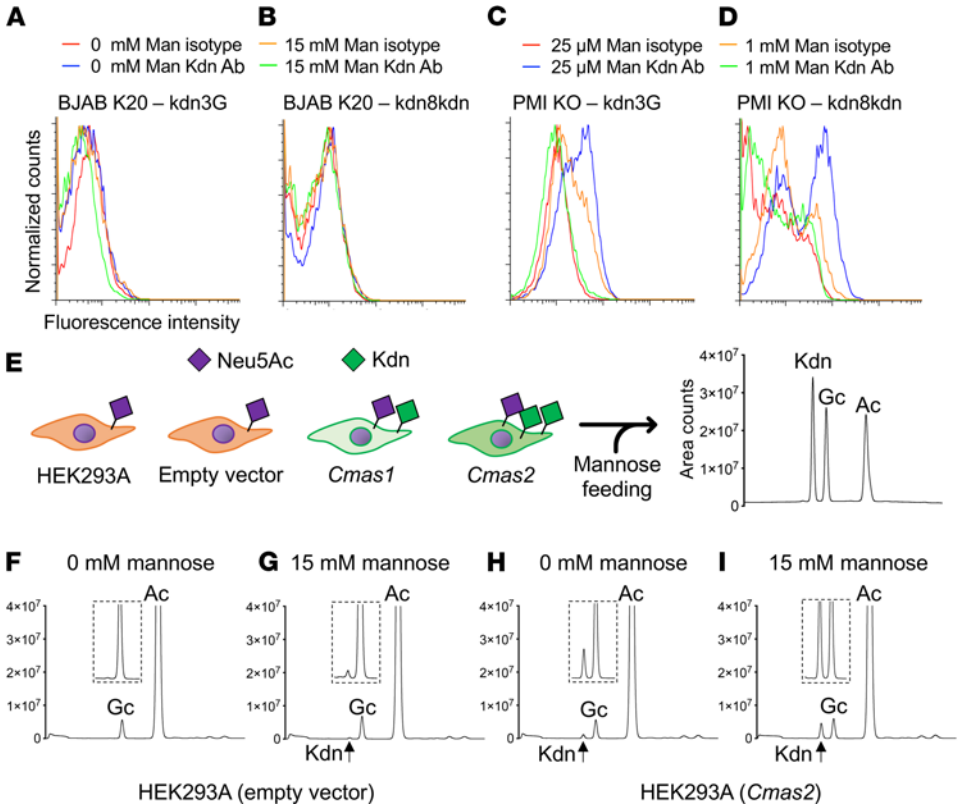

Figure 7. Gene mutations or fish *Cmas* transfection can enforce production of the conjugated form of Kdn. Mouse monoclonal anti–Kdn IgG antibody, with kdn3G recognizing the (Kdn) ganglioside GM3 and mouse monoclonal anti–Kdn IgM antibody, with kdn8kdn recognizing the α2,8-linked Kdn were used for flow cytometry to analyze cell-surface expression of Kdn. Results are shown for (**A** and **B**) BJAB K20 (GNE-KO) cells and (**C** and **D**) PMI-KO cells, with or without mannose feeding. (**E**) Empty vector, *Cmas1*, and *Cmas2* were transiently expressed in HEK293A cells. Cells were harvested after 36 hours of mannose feeding (0 or 15 mM), and then membrane fractions were prepared to analyze the conjugated form of Sia by DMB-HPLC analysis (Kdn, Neu5Gc, and Neu5Ac). Representative HPLC peaks for empty vector (**F** and **G**) or *Cmas2*-transfected (**H** and **I**) membrane samples. (**F** and **H**) 0 mM and (**G** and **I**) 15 mM mannose feeding. Data are representative of 2 independent experiments. Ac, Neu5Ac; Gc, Neu5Gc; Man, mannose.

activity toward Kdn since the relatively ancient divergence of warm- and cold-blooded vertebrates.

For a free monosaccharide to be incorporated into a glycan structure, it must first be activated to a high-energy donor, e.g., conjugated with a nt, and then transferred to a glycosyl acceptor. In humans, CMAS and sialyltransferases (STs) retain the enzyme promiscuity necessary to efficiently conjugate exogenous Neu5Gc to CMP-Neu5Gc and subsequently incorporate the xenogenic Sia into a "xeno-autoantigen" glycan structure. However, the pseudogenization of the human *CMAH* gene occurred relatively recently, after the divergence of humans and chimpanzees. Compared with Neu5Gc, the efficiency of Sia in activating and transferring enzymes toward Kdn seemed to be much lower, since we only detected trace amounts of glycan-conjugated Kdn in human and mouse cells cultured in high-mannose media compared with the efficient incorporation of Neu5Gc present in trace amounts in the FCS-supplemented media. In contrast, Kdn is found in abundance in fish glycoconjugates based on a Cmas paralog that has evolved preferential activity toward Kdn. Using a previously published expression construct (78), we show here that in vitro expression of the Kdn-active zebrafish Cmas enzyme forced the expression of small amounts of Kdn-containing cell-surface glycans also in HEK293A cells (Figure 7 and Supplemental Table 6), which normally excreted excess Kdn to maintain a constant cytosolic Kdn concentration (Figure 5 and Supplemental Table 3).

Free Neu5Ac or Kdn is synthesized by NANS from *N*-acetylmannosamine (ManNAc) or Man-6P and phosphoenolpyruvate, respectively. In vitro analyses showed that the biosynthetic activity of Kdn is based on methionine or leucine at position 42 in human NANS. In line with glycosidically conjugated Kdn, amphibia and fish NANS harbors methionine at position 42 (M42). Mouse NANS harbors the less active threonine (T42) and shows low Kdn biosynthesis in vitro (74). However, synthesis of free Kdn was observed in mouse cell culture in a high-mannose media, indicating residual enzymatic activity on Man-6P. Phylogenetic analyses showed that the common vertebrate ancestor harbors the Kdn-metabolizing M42, which is maintained mainly in nonmammalian classes and probably got lost during placentation in mammals (Figure 6). Reversion to methionine in placentals occurred independently by convergent evolution in primates and artiodactyla. Given these phylogenetic occurrences of Kdn biosynthetic enzymes, it is tempting to speculate that these orders might be more prone to a mannose-rich diet and/or lack microbiota capable of mannose uptake. Free Sias are catabolized by action of *N*-acetylneuraminate pyruvate lyase (NPL) in vivo. However, human NPL has a 5-fold lower activity on Neu5Gc compared with Neu5Ac and no detectable activity on Kdn (88), thus favoring the persistence of free Kdn.

Interestingly, the distribution of Kdn in tissues of fish such as Atlantic salmon vary between skin and intestinal mucins; *O*-glycan structures showed that Neu5Ac, Neu5Gc, and Kdn are distributed in skin mucin, however, intestinal mucin contains only Neu5Ac (89, 90). Perhaps different host-pathogen interactions between aquatic and terrestrial habitats and/or constant exposure to hydrophilic aqueous environments produced different evolutionary pressures on Sia presentation.

In this study, we explored why the conversion of mannose into Kdn has been conserved in mammals like humans, despite the lack of conclusive evidence of Kdn presence in sialoglycoconjugates. On the basis of our human experiments, we hypothesize that mannose is handled like glucose in the kidney, being reabsorbed in the tubules,

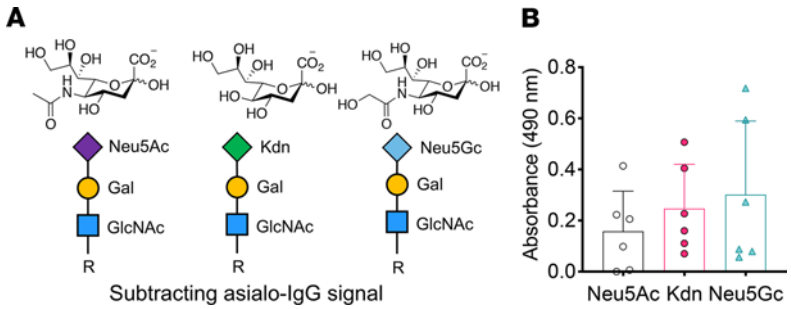

Figure 8. ELISA of anti-sialoglycan antibodies in human sera. (**A**) The chemoenzymatically synthesized, defined biotinylated glycans Neu5Acα2-3Galβ1-4GlcNAc-, Neu5Gcα2-3Galβ1-4GlcNAc-, Kdnα2-3Galβ1-4GlcNAc-biotin, respectively. (**B**) Anti-Sia antibodies (Neu5Ac, Kdn, and Neu5Gc) were detected in pooled normal human sera (IVIg) samples (n = 6 each). The absorbance of the wells coated with Galβ1-4GlcNAc- (negative control) glycan was subtracted from the corresponding sialoglycan-containing wells to determine the relative absorbance resulting from the specific anti-Sia antibodies. Data are shown as the mean (SD), and statistical significance was determined by 1-way ANOVA.

as previously reported (83, 91, 92), which implies that mannose is biologically "valuable." However, excess mannose could also be excreted into urine, just as occurs with excess glucose in patients with diabetes (direct mannose control, Figure 3A). Moreover, phylogenetic analysis of vertebrate Kdn synthesis, together with in vivo oral mannose administration and in vitro mannose feeding studies, suggested that excess exogenous mannose is transported into the cytosol, then metabolized to Kdn through the conserved metabolic pathway, excreted from the cells, and finally eliminated from the body through the urine (indirect mannose control). We confirmed by mannose supplementation in the media of different human (HEK293A, HUVEC, BJAB, HK2) as well as mouse (PMI) cell lines that mammalian cells very efficiently excreted cytosolic Kdn into the media (Supplemental Table 3). Furthermore, Man-6P was not detectable in human serum or urine even after mannose ingestion (Supplemental Figure 3), consistent with our hypothesis that Kdn synthesis helps minimize the buildup of toxic Man-6P in the cytosol under conditions of mannose excess. However, we speculate that this is not the only reason. For example, mannose is 5 times more reactive in detrimental nonenzymatic protein glycation than is glucose (93) and therefore needs to be regulated. Also, we recently found that free Kdn can compete with host Neu5Ac for uptake by commensal and/or pathogenic bacteria, affecting their interaction with host immunity (94).

Overall, our work can help explain the evolutionary conservation of Kdn biosynthesis throughout the higher vertebrate phylogeny. Even though higher vertebrates, including humans, do not utilize Kdn in glycoconjugate production, Kdn synthesis remains a critical metabolic pathway that buffers the potentially toxic concentration of cytosolic Man-6P and Fru-6P. Moreover, humans produce anti-Kdn antibodies, probably because of the presentation of Kdn-containing antigens originating from symbiotic flora, as has been observed with human anti-Neu5Gc antibodies (14, 94). Our findings regarding the Kdn/mannose pathway (Figure 1) may contribute to identifying the exact pathways by which Kdn is taken up into cells and tissues and by which humans produce anti-Kdn antibodies. Ultimately, deciphering the role of Kdn metabolism may lead to a better understanding of human diseases, including congenital disorders of glycosylation involving PMI, NANS, and NPL (88, 95, 96), as well as ESRD. It also remains possible that small amounts of conjugated Kdn may appear in tissues under pathological conditions like ESRD with high free Kdn levels and mediate inflammatory reactions with circulating anti–Kdn-glycan antibodies. If human cells are forced to incorporate small amounts of Kdn into surface glycans (e.g., under conditions of excess Kdn accumulation such as in acute or chronic uncontrolled renal failure), low levels of cell-surface accumulation could result in reactivity with such antibodies.

Methods

Human studies involving serum samples form patients with ESRD and healthy volunteer controls. Sera from patients with ESRD were collected just prior to weekly dialysis. Control samples were collected from healthy volunteers. All samples were anonymized, numbered, and kept at –80°C before analysis.

Human mannose ingestion test. Five informed and consented healthy volunteers ingested 0.2 g mannose/kg body weight dissolved in 500 mL drinking water, as previously tested (47). Blood samples (up to total 60 mL/person) were collected by venipuncture at 0, 1, 2, 4, 6, and 8 hours. Urine samples were collected as near as possible to the aforementioned times. All samples were analyzed for free and conjugated Kdn, Neu5Gc and Neu5Ac, as well as for mannose.

Cell culture and transfection. HEK293A cells (Thermo Fisher Scientific) were cultivated in RPMI 1640 media with 10% FBS; HUVECs (American Type Culture Collection [ATCC]) in EBM2 media (Lonza); BJAB K20 and BJAB K88 cells (provided by Stephan Hinderlich and the late Werner Reutter, Beuth University of Applied Sciences, Berlin, Germany) in RPMI 1640 media with 10% FBS; PMI WT and PMI-KO cells in DMEM containing 1 g/L glucose and 10% FBS; and HK2 cells in keratinocyte serum-free media supplemented with bovine pituitary extract and recombinant EGF (all from Gibco, Thermo Fisher Scientific). Transient transfection of *Cmas1* and *Cmas2* (and empty vector) was performed using polyethylenimine (PEI) at a final concentration of 18 μg/100 cm tissue culture dish and 8 μg plasmid DNA following standard protocols. The transfection media were removed after 4.5 hours, and the cells were incubated in complete media with or without added mannose at the indicated concentrations.

Cell viability measurement. Cell viability was measured using the RealTime-Glo MT Viability Assay (Promega) according to the instructions manual. Cells were incubated in culture media at various concentrations (25 μM–200 mM) of mannose or *N*-acetylglucosamine, which was used as a control for osmolarity effects. MT Cell Viability Substrate and NanoLuc enzymes (both from Promega) were also added to the culture, and viability was monitored by reading luminescence at 0, 12, 24, 36, 48, 60, 72, and 84 hours.

Cell fractionation and sodium borohydride treatment. Cell fractionation and borohydrate treatment were done as previously reported (64) and are detailed in the Supplemental Methods.

Detection of serum mannose levels by GC-MS. A 100 μL serum sample was spiked with 1 μg $^{13}C_6$-mannose as an internal standard, and 400 μL cold acetonitrile (–20°C) was added to precipitate the proteins. The sample was vortexed and kept on ice for 30 minutes to ensure

complete precipitation. The sample was then centrifuged at 14,000*g* at 4°C for 7 minutes, and the supernatant was removed and dried using a speed vac and lyophilizer. The dried samples were added to Tri-Sil Reagent (Thermo Fisher Scientific) and incubated at 80°C for 30 minutes. The reaction tube was then cooled to room temperature (RT), and excess reagent was removed by drying the samples. The Tri-Sil–derivatized sample was then dissolved in hexane and analyzed by GC-MS. Quantification was done by comparing the intensities of $^{12}C_6$ and $^{13}C_6$ mannose in the samples.

Detection of mannose in urine samples by GC-MS. Urine samples were centrifuged at 14,000*g* for 5 minutes at 10°C to remove any insoluble material. A 1 mL urine sample was spiked with 1 μg $^{13}C_6$-mannose as an internal standard and passed over preconditioned LC-NH2 SPE tubes (Supelco), and the flow-through was collected. The LC-NH2 SPE tubes were further washed with 1 mL ultrapure water, and the dried flow-through products were then re-dissolved in 1 mL water, transferred into a screw-capped glass reaction tube, and dried in a lyophilizer. Tri-Sil HTP Reagent (250 μL , Thermo Fisher Scientific) was added on the dried sample, sonicated (10–15 s), and reacted at 80°C for 30 minutes. Tri-Sil–derivatized samples were then extracted by adding 1.5 mL hexane followed by sonication, vortexing, and filtration using a glass wool fiber–packed glass Pasteur pipette. The filtrate was dried and placed in the GC-MS autosampler vial. GC-MS analysis was performed in EI mode using the Restek-5MS glass capillary column (30 mL, 25 mm inner diameter [ID]). Identification of mannose was done from the retention time of mannose on the column and quantified by comparing the ratio of ion intensities (*m/z* of 204:206) of the corresponding fragment mass from $^{12}C_6$ and $^{13}C_6$ mannose.

Detection of serum/urine Sia levels by HPLC. Serum samples (250 μL) were spun at 20,000*g* for 10 minutes and filtered, and the DMB-derivatized samples were then analyzed by HPLC as previously described (97). Cold acetonitrile (400 μL, –20°C) was added to a 100 μL urine sample and kept on ice for 30 minutes. The sample was then centrifuged at 14,000*g* at 4°C for 7 minutes, and the supernatant was passed through a 3K spin filter. The flow-through was dried, DMB-tagged, and detected using HPLC–fluorescence detector (HPLC-FL) under isocratic solvent conditions (same as for Sia tagging).

Flow cytometry. Cells were blocked with 1% BSA in PBS and stained with mouse anti-Kdn antibodies on ice for 30 minutes. Following primary antibody staining, the cells were washed and stained with APC-conjugated anti-mouse antibody (Poly4053, BioLegend). Anti–Flag-F3165 (MilliporeSigma) was used to measure the population of *Cmas*-transfected HEK293A cells. Acquisition and analysis were performed using the BD FACSCalibur and FlowJo software, respectively.

Sequence alignments, tests for selection, and the phylogenetic tree. Coding nt and aa sequences of mannose metabolism genes and proteins were obtained from the NCBI's nt and protein databases. Nucleotide alignments and the percentage of identity were produced using the NCBI's Basic Local Alignment Search Tool (BLAST) (https://blast.ncbi.nlm.nih.gov/Blast.cgi). Protein sequences were aligned using the Clustal Omega program (UniProt.org). Nucleotide alignments were used to analyze the ratio of nonsynonymous (Ka) to synonymous (Ks) substitution, evaluated with an online calculation tool (http://services.cbu.uib.no/tools/kaks). The Ka/Ks ratio is representative of purifying selection on a coding sequence, as a Ka/Ks of less than 1 indicates that there is pressure to conserve the amino sequence relative to the background mutation rate. A maximum likelihood tree was constructed using the general time reversible model (98). The tree with the highest log likelihood is shown. Initial trees for the heuristic search were obtained automatically by applying the maximum parsimony method. A discrete γ distribution was used to model evolutionary rate differences among sites (5 categories, +gamma distribution [+G], parameter = 0.6749). The rate variation model allowed for some sites to be evolutionarily invariable ([+invariance] (+I), 21.44% sites).

Detection of anti-Sia antibodies in pooled human intravenous Ig. Intravenous Ig (IVIg) was used for the detection of anti-Sia antibodies (Kdn, Neu5Gc, Neu5Ac). Briefly, a 96-well plate (CoStar) was coated overnight with 100 μg/mL streptavidin at 4°C and washed with PBS containing 0.1% Tween 20 (PBST). The chemoenzymatically synthesized, defined glycans were used to determine the presence of antibodies against a specific glycan structure. The glycan epitopes used were Neu5Acα2-3Galβ1-4GlcNAc-, Neu5Gcα2-3Galβ1-4GlcNAc-, Kdnα2-3Galβ1-4GlcNAc-, and unsialylated Galβ1-4GlcNAc- (negative control). Each of these glycans was biotinylated. Following streptavidin coating, the wells were further blocked with PBST for 1.5 hours at RT and coated with 500 ng of the respective biotinylated glycan per well for 2 hours. Following incubation, the wells were washed with PBST and incubated with IVIg (1:250 dilution) for 1.5 hours at RT. Finally, the wells were washed and incubated with HRP-conjugated goat anti–human IgG antibodies (catalog 172-1050, Bio-Rad, 1:10,000 dilution) for 1 hour, and then washed and visualized at 490 nm following HRP substrate addition. For quantification of intensity resulting from the specific antibodies against Neu5Ac/Neu5Gc/Kdn epitopes and not from any nonspecific antibodies against the underlying glycan structure, the absorbance of the unsialylated conditions (wells coated with Galβ1-4GlcNAc- glycans) was subtracted from the corresponding values of the sialoglycan-coated wells.

Statistics. Data were analyzed by *t* test or ANOVA, as indicated in the figure legends, and are presented as the mean (SD) using GraphPad Prism software, version 9 (GraphPad Software). *P* values of less than 0.05 were considered significant.

Study approval. Human sample collection was approved by the UCSD Human Research Protections Program (HRPP) (111279XX). Informed consent was obtained from all participants prior to sample collection. Ethics approval for the human mannose ingestion study was obtained from the UCSD HRPP (172014X).

Author contributions

AV conceptualized the study. K. Kawanishi, SS, SD, AS, BC, AMK, and AV designed the study methodology. SS and MV validated the findings. K. Kawanishi, SD, MV, AS, SSS, BC, and AMK conducted formal analysis. K. Kawanishi, SS, SD, MV, AS, SSS, BC, and AMK performed experiments. ICS, CS, K. Kitajima, KS, HHF, AMK, and AV provided resources. K. Kawanishi and AV wrote the original draft of the manuscript. K. Kawanishi, SS, SD, MV, XC, HHF, AMK, and AV reviewed and edited the manuscript. K. Kawanishi, SS, MV, SSS, AS, and AMK performed visualization of the data. HHF, AMK, and AV supervised the study. AV was responsible for project administration. HHF, and AV acquired funding for the study. K. Kawanishi designed study methodology, performed experiments, visualization of the data, and formal analysis, and wrote the original draft and reviewed and edited the manuscript. SS designed study methodology and performed data validation, experiments, visualization of the data, and reviewed and edited the manuscript.

Acknowledgments

This work was supported primarily by NIH grant R01GM32373 (to AV) and by the Rocket Fund and NIH grant R01DK99551 (to HHF), as well as by AMED grant 20ae0101069h0005 (to CS) and DFG grant MU 1849/3-1 (to AMK). MV was supported in part by a Ruth L. Kirschstein Institutional National Research Award from the National Institute for General Medical Sciences, by the UCSD Genetics Training Program (T32 GM008666), and by a Training Grant in Gastroenterology (DK007202).

Address correspondence to: Ajit Varki, University of California, San Diego, 9500 Gilman Drive, La Jolla, California 92093-0687, USA. Phone: 858.534.2214; Email: a1varki@health.ucsd.edu. K. Kawanishi's present address is: Kidney and Vascular Pathology, Faculty of Medicine, University of Tsukuba, Ibaraki, Japan. SSS's present address is: American University of Ras Al Khaimah (AURAK), United Arab Emirates (UAE). KS's present address is: Center for Renal Precision Medicine, Division of Nephrology, Department of Medicine, University of Texas Health San Antonio, San Antonio, Texas, USA. SSS's present address is: School of Life and Medical Sciences, University of Hertfordshire, College Lane Campus, Hatfield, United Kingdom. CS's present address is: Institute for Glyco-core Research, Nagoya University, and Graduate School of Bioagricultural Sciences, Nagoya University, Nagoya, Japan. K. Kitajima' present address is: Institute for Glyco-core Research, Nagoya University, Nagoya University, Nagoya, Japan.

1. Kelm S, Schauer R. Sialic acids in molecular and cellular interactions. *Int Rev Cytol*. 1997;175:137–240.
2. Varki A. Glycan-based interactions involving vertebrate sialic-acid-recognizing proteins. *Nature*. 2007;446(7139):1023–1029.
3. Schnaar RL, et al. Sialic acids in the brain: gangliosides and polysialic acid in nervous system development, stability, disease, and regeneration. *Physiol Rev*. 2014;94(2):461–518.
4. Pearce OM, Läubli H. Sialic acids in cancer biology and immunity. *Glycobiology*. 2016;26(2):111–128.
5. Schauer R, Kamerling JP. Exploration of the sialic acid world. *Adv Carbohydr Chem Biochem*. 2018;75:1–213.
6. Varki A. Sialic acids in human health and disease. *Trends Mol Med*. 2008;14(8):351–360.
7. von Gunten S , Bochner BS . Basic and clinical immunology of Siglecs. *Ann N Y Acad Sci*. 2008;1143:61–82.
8. Lewis AL, Lewis WG. Host sialoglycans and bacterial sialidases: a mucosal perspective. *Cell Microbiol*. 2012;14(8):1174–1182.
9. Wasik BR, et al. Effects of sialic acid modifications on virus binding and infection. *Trends Microbiol*. 2016;24(12):991–1001.
10. Zhou JY, et al. The glycoscience of immunity. *Trends Immunol*. 2018;39(7):523–535.
11. Chou HH, et al. Inactivation of CMP-N-acetylneuraminic acid hydroxylase occurred prior to brain expansion during human evolution. *Proc Natl Acad Sci U S A*. 2002;99(18):11736–11741.
12. Padler-Karavani V, et al. Cross-comparison of protein recognition of sialic acid diversity on two novel sialoglycan microarrays. *J Biol Chem*. 2012;287(27):22593–22608.
13. Samraj AN, et al. Polyclonal human antibodies against glycans bearing red meat-derived non-human sialic acid N-glycolylneuraminic acid are stable, reproducible, complex and vary between individuals: Total antibody levels are associated with colorectal cancer risk. *PLoS One*. 2018;13(6):e0197464.
14. Taylor RE, et al. Novel mechanism for the generation of human xeno-autoantibodies against the nonhuman sialic acid *N*-glycolylneuraminic acid. *J Exp Med*. 2010;207(8):1637–1646.
15. Tangvoranuntakul P, et al. Human uptake and incorporation of an immunogenic nonhuman dietary sialic acid. *Proc Natl Acad Sci U S A*. 2003;100(21):12045–12050.
16. Varki NM, et al. Biomedical differences between human and nonhuman hominids: potential roles for uniquely human aspects of sialic acid biology. *Annu Rev Pathol*. 2011;6:365–393.
17. Samraj AN, et al. Involvement of a non-human sialic acid in human cancer. *Front Oncol*. 2014;4:33.
18. Ma F, et al. A mouse model for dietary xenosialitis: antibodies to xenoglycan can reduce fertility. *J Biol Chem*. 2016;291(35):18222–18231.
19. Amon R, et al. Glycan microarray reveal induced IgGs repertoire shift against a dietary carbohydrate in response to rabbit anti-human thymocyte therapy. *Oncotarget*. 2017;8(68):112236–112244.
20. Samraj AN, et al. A red meat-derived glycan promotes inflammation and cancer progression. *Proc Natl Acad Sci U S A*. 2015;112(2):542–547.
21. Kawanishi K, et al. Human species-specific loss of CMP-*N*-acetylneuraminic acid hydroxylase enhances atherosclerosis via intrinsic and extrinsic mechanisms. *Proc Natl Acad Sci U S A*. 2019;116(32):16036–16045.
22. Nadano D, et al. A naturally occurring deaminated neuraminic acid, 3-deoxy-D-glycero-D-galacto-nonulosonic acid (KDN). Its unique occurrence at the nonreducing ends of oligosialyl chains in polysialoglycoprotein of rainbow trout eggs. *J Biol Chem*. 1986;261(25):11550–11557.
23. Inoue S, et al. Identification of 2-keto-3-deoxy-D-glycero-D-galactonononic acid (KDN, deaminoneuraminic acid) residues in mammalian tissues and human lung carcinoma cells. *J Biol Chem*. 1996;271(40):24341–24344.
24. Chen Y, et al. LC-MS/MS quantification of N-acetylneuraminic acid, N-glycolylneuraminic acid and ketodeoxynonulosonic acid levels in the urine and potential relationship with dietary sialic acid intake and disease in 3- to 5-year-old children. *Br J Nutr*. 2014;111(2):332–341.
25. Jahan M, et al. Molecular characterization of the level of sialic acids N-acetylneuraminic acid, N-glycolylneuraminic acid, and ketodeoxynonulosonic acid in porcine milk during lactation. *J Dairy Sci*. 2016;99(10):8431–8442.
26. Inoue S, et al. Identification and partial characterization of soluble and membrane-bound KDN(deaminoneuraminic acid)-glycoproteins in human ovarian teratocarcinoma PA-1, and enhanced expression of free and bound KDN in cells cultured in mannose-rich media. *Glycoconj J*. 2006;23(5–6):401–410.
27. Wang F, et al. LC-MS/MS glycomic analyses of free and conjugated forms of the sialic acids, Neu5Ac, Neu5Gc and KDN in human throat cancers. *Glycobiology*. 2015;25(12):1362–1374.
28. Yabu M, et al. Occurrence of free deaminoneuraminic acid (KDN)-containing complex-type N-glycans in human prostate cancers. *Glycobiology*. 2013;23(6):634–642.
29. Kanamori A, et al. Monoclonal antibody specific for alpha 2→8-linked oligo deaminated neuraminic acid (KDN) sequences in glycoproteins. Preparation and characterization of a monoclonal antibody and its application in immunohistochemistry. *Histochemistry*. 1994;101(5):333–340.
30. Ziak M, et al. Occurrence of poly(alpha2,8-deaminoneuraminic acid) in mammalian tissues: widespread and developmentally regulated but highly selective expression on glycoproteins. *Proc Natl Acad Sci U S A*. 1996;93(7):2759–2763.
31. Ziak M, Roth J. Expression of oligo/polyalpha2,8-linked deaminoneuraminic acid and megalin during kidney development and maturation: mutually exclusive distribution with polyalpha2,8-linked N-acetylneuraminic acid of N-CAM. *Histochem Cell Biol*. 1999;112(2):169–178.
32. Ziak M, et al. Identification of megalin as the sole rat kidney sialoglycoprotein containing poly alpha2,8 deaminoneuraminic acid. *J Am Soc Nephrol*. 1999;10(2):203–209.
33. Ziak M, et al. Megalin in normal tissues and carcinoma cells carries oligo/poly alpha2,8 deaminoneuraminic acid as a unique posttranslational modification. *Glycoconj J*. 1999;16(3):185–188.
34. Ziak M, et al. Ceruloplasmin carries the anionic glycan oligo/poly alpha2,8 deaminoneuraminic acid. *Biochem Biophys Res Commun*. 2002;295(3):597–602.
35. Angata T, et al. Elevated expression of free deaminoneuraminic acid in mammalian cells cultured in mannose-rich media. *Biochem Biophys Res Commun*. 1999;261(2):326–331.
36. Go S, et al. Oral ingestion of mannose alters the expression level of deaminoneuraminic acid (KDN) in mouse organs. *Glycoconj J*. 2006;23(5-6):411–421.
37. Etchison JR, Freeze HH. Enzymatic assay of D-mannose in serum. *Clin Chem*. 1997;43(3):533–538.
38. Panneerselvam K, Freeze HH. Mannose enters mammalian cells using a specific transporter

that is insensitive to glucose. *J Biol Chem*. 1996;271(16):9417–9421.
39. Ichikawa M, et al. The metabolic origins of mannose in glycoproteins. *J Biol Chem*. 2014;289(10):6751–6761.
40. DeRossi C, et al. Ablation of mouse phosphomannose isomerase (Mpi) causes mannose 6-phosphate accumulation, toxicity, and embryonic lethality. *J Biol Chem*. 2006;281(9):5916–5927.
41. de Lonlay P, et al. Hyperinsulinemic hypoglycemia as a presenting sign in phosphomannose isomerase deficiency: a new manifestation of carbohydrate-deficient glycoprotein syndrome treatable with mannose. *J Pediatr*. 1999;135(3):379–383.
42. Niehues R, et al. Carbohydrate-deficient glycoprotein syndrome type Ib. Phosphomannose isomerase deficiency and mannose therapy. *J Clin Invest*. 1998;101(7):1414–1420.
43. Sols A, et al. Enzymatic basis of mannose toxicity in honey bees. *Science*. 1960;131(3396):297–298.
44. de la Fuente M, et al. Mechanism of mannose toxicity. *Biochem Biophys Res Commun*. 1986;140(1):51–55.
45. Sharma V, et al. Mannose supplements induce embryonic lethality and blindness in phosphomannose isomerase hypomorphic mice. *FASEB J*. 2014;28(4):1854–1869.
46. Sharma V, et al. Mannose metabolism: more than meets the eye. *Biochem Biophys Res Commun*. 2014;453(2):220–228.
47. Alton G, et al. Oral ingestion of mannose elevates blood mannose levels: a first step toward a potential therapy for carbohydrate-deficient glycoprotein syndrome type I. *Biochem Mol Med*. 1997;60(2):127–133.
48. Kranjcec B, et al. D-mannose powder for prophylaxis of recurrent urinary tract infections in women: a randomized clinical trial. *World J Urol*. 2014;32(1):79–84.
49. Foxman B. The epidemiology of urinary tract infection. *Nat Rev Urol*. 2010;7(12):653–660.
50. Aronson M, et al. Prevention of colonization of the urinary tract of mice with Escherichia coli by blocking of bacterial adherence with methyl alpha-D-mannopyranoside. *J Infect Dis*. 1979;139(3):329–332.
51. Zhang D, et al. D-mannose induces regulatory T cells and suppresses immunopathology. *Nat Med*. 2017;23(9):1036–1045.
52. Sharma V, et al. Mannose alters gut microbiome, prevents diet-induced obesity, and improves host metabolism. *Cell Rep*. 2018;24(12):3087–3098.
53. Lee S, et al. Integrated network analysis reveals an association between plasma mannose levels and insulin resistance. *Cell Metab*. 2016;24(1):172–184.
54. Yoshimura K, et al. Plasma mannose level, a putative indicator of glycogenolysis, and glucose tolerance in Japanese individuals. *J Diabetes Investig*. 2017;8(4):489–495.
55. Mardinoglu A, et al. Plasma mannose levels are associated with incident type 2 diabetes and cardiovascular disease. *Cell Metab*. 2017;26(2):281–283.
56. Long Y, et al. Global and targeted serum metabolic profiling of colorectal cancer progression. *Cancer*. 2017;123(20):4066–4074.
57. Gonzalez PS, et al. Mannose impairs tumour growth and enhances chemotherapy. *Nature*. 2018;563(7733):719–723.
58. Nöhle U, et al. Uptake, metabolism and excretion of orally and intravenously administered, double-labeled N-glycoloylneuraminic acid and single-labeled 2-deoxy-2,3-dehydro-N-acetylneuraminic acid in mouse and rat. *Eur J Biochem*. 1982;126(3):543–548.
59. Banda K, et al. Metabolism of vertebrate amino sugars with N-glycolyl groups: mechanisms underlying gastrointestinal incorporation of the non-human sialic acid xeno-autoantigen N-glycolylneuraminic acid. *J Biol Chem*. 2012;287(34):28852–28864.
60. Pham T, et al. Evidence for a novel human-specific xeno-auto-antibody response against vascular endothelium. *Blood*. 2009;114(25):5225–5235.
61. Alton G, et al. Direct utilization of mannose for mammalian glycoprotein biosynthesis. *Glycobiology*. 1998;8(3):285–295.
62. Hinderlich S, et al. Biosynthesis of N-acetylneuraminic acid in cells lacking UDP-N-acetylglucosamine 2-epimerase/N-acetylmannosamine kinase. *Biol Chem*. 2001;382(2):291–297.
63. Denzel MS, et al. Hexosamine pathway metabolites enhance protein quality control and prolong life. *Cell*. 2014;156(6):1167–1178.
64. Seppala R, et al. Sialic acid metabolism in sialuria fibroblasts. *J Biol Chem*. 1991;266(12):7456–7461.
65. Ryan MJ, et al. HK-2: an immortalized proximal tubule epithelial cell line from normal adult human kidney. *Kidney Int*. 1994;45(1):48–57.
66. Antonopoulos A, et al. Glycosylation of mouse and human immune cells: insights emerging from N-glycomics analyses. *Biochem Soc Trans*. 2011;39(5):1334–1340.
67. Altheide TK, et al. System-wide genomic and biochemical comparisons of sialic acid biology among primates and rodents: evidence for two modes of rapid evolution. *J Biol Chem*. 2006;281(35):25689–25702.
68. Hao J, et al. Elimination of 2-keto-3-deoxy-D-glycero-D-galacto-nonulosonic acid 9-phosphate synthase activity from human N-acetylneuraminic acid 9-phosphate synthase by a single mutation. *Biochem J*. 2006;397(1):195–201.
69. Song Y, et al. Monoclonal antibody specific to alpha-2→3-linked deaminated neuraminyl beta-galactosyl sequence. *Glycobiology*. 1993;3(1):31–36.
70. Sato C, et al. Characterization of the antigenic specificity of four different anti-(alpha 2→8-linked polysialic acid) antibodies using lipid-conjugated oligo/polysialic acids. *J Biol Chem*. 1995;270(32):18923–18928.
71. Whitman CM, et al. Modified GM3 gangliosides produced by metabolic oligosaccharide engineering. *Bioorg Med Chem Lett*. 2011;21(17):5006–5010.
72. Pham ND, et al. Effects of altered sialic acid biosynthesis on *N*-linked glycan branching and cell surface interactions. *J Biol Chem*. 2017;292(23):9637–9651.
73. Lawrence SM, et al. Cloning and expression of the human N-acetylneuraminic acid phosphate synthase gene with 2-keto-3-deoxy-D-glycero-D-galacto-nononic acid biosynthetic ability. *J Biol Chem*. 2000;275(23):17869–17877.
74. Nakata D, et al. Molecular cloning and expression of the mouse N-acetylneuraminic acid 9-phosphate synthase which does not have deaminoneuraminic acid (KDN) 9-phosphate synthase activity. *Biochem Biophys Res Commun*. 2000;273(2):642–648.
75. Nakata D, et al. Molecular cloning of a unique CMP-sialic acid synthetase that effectively utilizes both deaminoneuraminic acid (KDN) and N-acetylneuraminic acid (Neu5Ac) as substrates. *Glycobiology*. 2001;11(8):685–692.
76. Lawrence SM, et al. Cloning and expression of human sialic acid pathway genes to generate CMP-sialic acids in insect cells. *Glycoconj J*. 2001;18(3):205–213.
77. Pasquier J, et al. Gene evolution and gene expression after whole genome duplication in fish: the PhyloFish database. *BMC Genomics*. 2016;17:368.
78. Schaper W, et al. Identification and biochemical characterization of two functional CMP-sialic acid synthetases in Danio rerio. *J Biol Chem*. 2012;287(16):13239–13248.
79. Padler-Karavani V, et al. Diversity in specificity, abundance, and composition of anti-Neu5Gc antibodies in normal humans: potential implications for disease. *Glycobiology*. 2008;18(10):818–830.
80. Herman RH. Mannose metabolism. I. *Am J Clin Nutr*. 1971;24(4):488–498.
81. Sharma V, Freeze HH. Mannose efflux from the cells: a potential source of mannose in blood. *J Biol Chem*. 2011;286(12):10193–10200.
82. De la Horra MC, et al. Na(+)-dependent D-mannose transport at the apical membrane of rat small intestine and kidney cortex. *Biochim Biophys Acta*. 2001;1512(2):225–230.
83. Grempler R, et al. Functional characterisation of human SGLT-5 as a novel kidney-specific sodium-dependent sugar transporter. *FEBS Lett*. 2012;586(3):248–253.
84. Mueckler M, Thorens B. The SLC2 (GLUT) family of membrane transporters. *Mol Aspects Med*. 2013;34(2–3):121–138.
85. Ono S, et al. Environment-dependent conformation and antimicrobial activity of a gramicidin S analog containing leucine and lysine residues. *FEBS Lett*. 1987;220(2):332–336.
86. Freinkel N, et al. The honeybee syndrome — implications of the teratogenicity of mannose in rat-embryo culture. *N Engl J Med*. 1984;310(4):223–230.
87. Buchanan T, et al. Fuel-mediated teratogenesis. Use of D-mannose to modify organogenesis in the rat embryo in vivo. *J Clin Invest*. 1985;75(6):1927–1934.
88. Wen XY, et al. Sialic acid catabolism by N-acetylneuraminate pyruvate lyase is essential for muscle function. *JCI Insight*. 2018;3(24):e122373.
89. Jin C, et al. Atlantic salmon carries a range of novel O-glycan structures differentially localized on skin and intestinal mucins. *J Proteome Res*. 2015;14(8):3239–3251.
90. Padra JT, et al. Aeromonas salmonicida growth in response to atlantic salmon mucins differs between epithelial sites, is governed by sialylated and *N*-acetylhexosamine-containing *O*-glycans, and is affected by Ca^2. *Infect Immun*. 2017;85(8):e00189–17.
91. Yamanouchi T, et al. Common reabsorption system of 1,5-anhydro-D-glucitol, fructose, and mannose in rat renal tubule. *Biochim Biophys*

Acta. 1996;1291(1):89–95.
92. Blasco T, et al. Expression and molecular characterization of rat renal D-mannose transport in Xenopus oocytes. *J Membr Biol*. 2000;178(2):127–135.
93. Bunn HF, Higgins PJ. Reaction of monosaccharides with proteins: possible evolutionary significance. *Science*. 1981;213(4504):222–224.
94. Saha S, et al. Exploring the impact of ketodeoxynonulosonic acid in host-pathogen interactions using uptake and surface display by non-typeable Haemophilus influenzae [published online January 19, 2021]. *mBio*. https://mbio.asm.org/content/12/1/e03226-20.
95. Tarailo-Graovac M, et al. Exome sequencing and the management of neurometabolic disorders. *N Engl J Med*. 2016;374(23):2246–2255.
96. van Karnebeek CD, et al. NANS-mediated synthesis of sialic acid is required for brain and skeletal development. *Nat Genet*. 2016;48(7):777–784.
97. Inoue S, et al. An ultrasensitive chemical method for polysialic acid analysis. *Glycobiology*. 2001;11(9):759–767.
98. Nei M, Kumar S. *Molecular Evolution and Phylogenetics*. Oxford University Press; 2000.
99. York WS, et al. GlyGen: computational and informatics resources for glycoscience. *Glycobiology*. 2020;30(2):72–73.
100. Alocci D, et al. GlyConnect: glycoproteomics goes visual, interactive, and analytical. *J Proteome Res*. 2019;18(2):664–677.
101. Campbell MP, et al. Validation of the curation pipeline of UniCarb-DB: building a global glycan reference MS/MS repository. *Biochim Biophys Acta*. 2013;1844(1 Pt A):108–116.
102. Taguchi R, et al. Basic analytical systems for lipidomics by mass spectrometry in Japan. *Methods Enzymol*. 2007;432:185–211.
103. Tiemeyer M, et al. GlyTouCan: an accessible glycan structure repository. *Glycobiology*. 2017;27(10):915–919.

Supplemental materials for

Evolutionary Conservation of human ketodeoxynonulosonic acid production is independent of sialoglycan biosynthesis

Kunio Kawanishi[1,2#*], Sudeshna Saha[1,2*], Sandra Diaz[1,2], Michael Vaill[1,2,3], Aniruddha Sasmal[1,2], Shoib S. Siddiqui[1,2##], Biswa Choudhury[1], Kumar Sharma[4###], Xi Chen[5], Ian C. Schoenhofen[6], Chihiro Sato[7], Ken Kitajima[7], Hudson H. Freeze[8], Anja Münster-Kühnel[9], and Ajit Varki[1, 2, 3, 4**].

[1]Glycobiology Research and Training Center, [2]Department of Cellular & Molecular Medicine, [3]Center for Academic Research and Training in Anthropogeny, and [4]Department of Medicine, University of California, San Diego, La Jolla, CA, USA.

[5]Department of Chemistry, University of California, Davis, Davis, CA, USA

[6]Human Health Therapeutics Research Center, National Research Council of Canada, Ottawa, Ontario, K1A 0R6, Canada,

[7]Bioscience and Biotechnology Center, Nagoya University, Nagoya, Japan.

[8]Human Genetics Program, Sanford Burnham Prebys Medical Discovery Institute, La Jolla, CA, USA.

[9] Clinical Biochemistry, Hannover Medical School, Hannover, Germany.

* The contributions of the first two authors are considered equal.

[#]Current Address: Kidney and Vascular Pathology, Faculty of Medicine, University of Tsukuba, Ibaraki, Japan

[##]Current Address: American University of Ras Al Khaimah (AURAK), United Arab Emirates (UAE)

[###]Current Address: Center for Renal Precision Medicine, Division of Nephrology, Department of Medicine, University of Texas Health San Antonio

**Correspondence: a1varki@health.ucsd.edu, University of California, San Diego, 9500 Gilman Drive, La Jolla, CA 92093-0687, USA.

Conflict of interest: The authors have declared that no conflict of interest exist.

Supplemental Materials and Methods

Detection of free α-ketoacids including sialic acids and by LC-MS. Analyses of α-ketoacids including Kdn, Neu5Ac, Neu5Gc (Supplemental Table 1) were done using LTQ-Orbitrap Discovery (Thermo Scientific) mass spectrometry attached to Ultimate3000 HPLC system (Thermo-Dionex) after tagging with DMB. The profiling of α-ketoacids was done using Phalanx C18 column (150mm x 1.0mm, 5µm) from Higgins Analytical. A step-gradient of solvents at a flow rate of 50 µL was used to get optimal separation between the sugar moieties. 5% aqueous methanol containing 0.1% formic acid was used as Solvent-A and mixture of 5% methanol, 45% water and 50% acetonitrile containing 0.1% formic acid was used as Solvent-B; the details of gradient is as follows. For 0-5 min mixture of 83% of solvent-A and 17% of solvent-B; for 5.1-10min 80% of solvent-A and 20% of solvent-B; for 10.1 to 15min 75% of solvent-A and 25% of solvent-B was used; for 15.1-20 min 70% of solvent-A and 30% of solvent-B is used and finally from 20.1-25min 50% solvent-A and 50% solvent-B was used. The mass spectral data was obtained in positive mode.

Sequence alignments, tests for selection and phylogenetic tree. Evolutionary analyses of NANS were conducted in MEGA X (Kumar S, Stecher G, Li M, Knyaz C, and Tamura K (2018) MEGA X: Molecular Evolutionary Genetics Analysis across computing platforms. Molecular Biology and Evolution 35:1547-1549). Information about sequences are given in Supplemental Table 8. Multiple alignment based on NANS nucleotide sequences was performed using MUSCLE with UPGMA algorithm.

Detection of Man-6P in human serum and urine by HPAEC-PAD. The frozen serum and urine samples were thawed and centrifuged at 3,000 rpm for 5 min at 4°C. Samples were divided into two 500 µL aliquots and one of them was added Man-6P (0.2 µg total per sample). Then the samples were filtered by Microcon-3 filter at 14,000 X g for 20 min at 4°C. Next, the flow through was passed over 1mL column packed with Dowex cation exchange resin (AG 50W-X8, 200-400 mesh). Then the resin was washed with 1 mL ultrapure water and the flow through was collected for Man-6P analysis using HPAEC-PAD (Dionex ICS-3000). Carbopac PA-1 column (Dionex CarboPac PA1 column 4 mm x 250 mm, 4µm, with a 4 mm x 50 mm Guard) was used for

monosaccharide profiling with 100 mM NaOH and 250 mM NaOAc as gradient mixture. Quantification was done by comparing with the known quantity of standard monosaccharides purchased from Sigma.

Cell fractionation and sodium borohydride treatment. Cells and media were collected after incubation with mannose. The media was centrifugated and 1.5 mL aliquot was passed filtered through a Microcon-10 filter and lyophilized. Cells were harvested with 10mM EDTA and washed with PBS; suspension cells were directly washed with PBS. Hereon all fractions are kept on ice. The cell pellets were lysed using ice cold water which had been titrated to pH 7.5 with 1M NH_4OH (for preservation of CMP-glycans) and sonicated with two 15 second bursts, with 15 second rest in-between. The homogenates were centrifuged at 100,000 g for 1 hour. The supernatant was collected, adjusted to 87.5% ethanol and centrifuged at 20,000 g for 10 min. The resulting supernatant was diluted to 10 % ethanol (using pH 7.5 water), frozen and lyophilized; this fraction was called FSF (Free-Sugar Fraction) containing Neu5Ac, Kdn, CMP-Neu5Ac, CMP-Kdn. The resulting pellet was called SPF (Soluble Protein Fraction) and was stored at -80˚C. The cell pellet was washed once with 3 mL cold water pH 7.5, sonicated, and centrifugation at 100,000 g for 1 hour. The membrane pellet was suspended in 200 µL water pH 7.5. Sodium borohydride treatment was performed on 25 µL of the FSF and media (after lyophilization, the dried material was dissolved in 200 µL ice-cold water). The sample was mixed with 25 µL of 0.5 M $NaBH_4$, incubated at 37˚C for 15 min, and quenched with 25 µL 5 M acetic acid, for 5 min at 4˚C and 10 min at37˚C. Control samples which were not subjected to borohydride treatment, had 25 µL of water added, 25 µL 5 M acetic acid, and incubated on ice for the first 20 min, and finished with 10 min incubation at 37˚C. The pH of each reaction was monitored.

Supplemental Figures and Tables

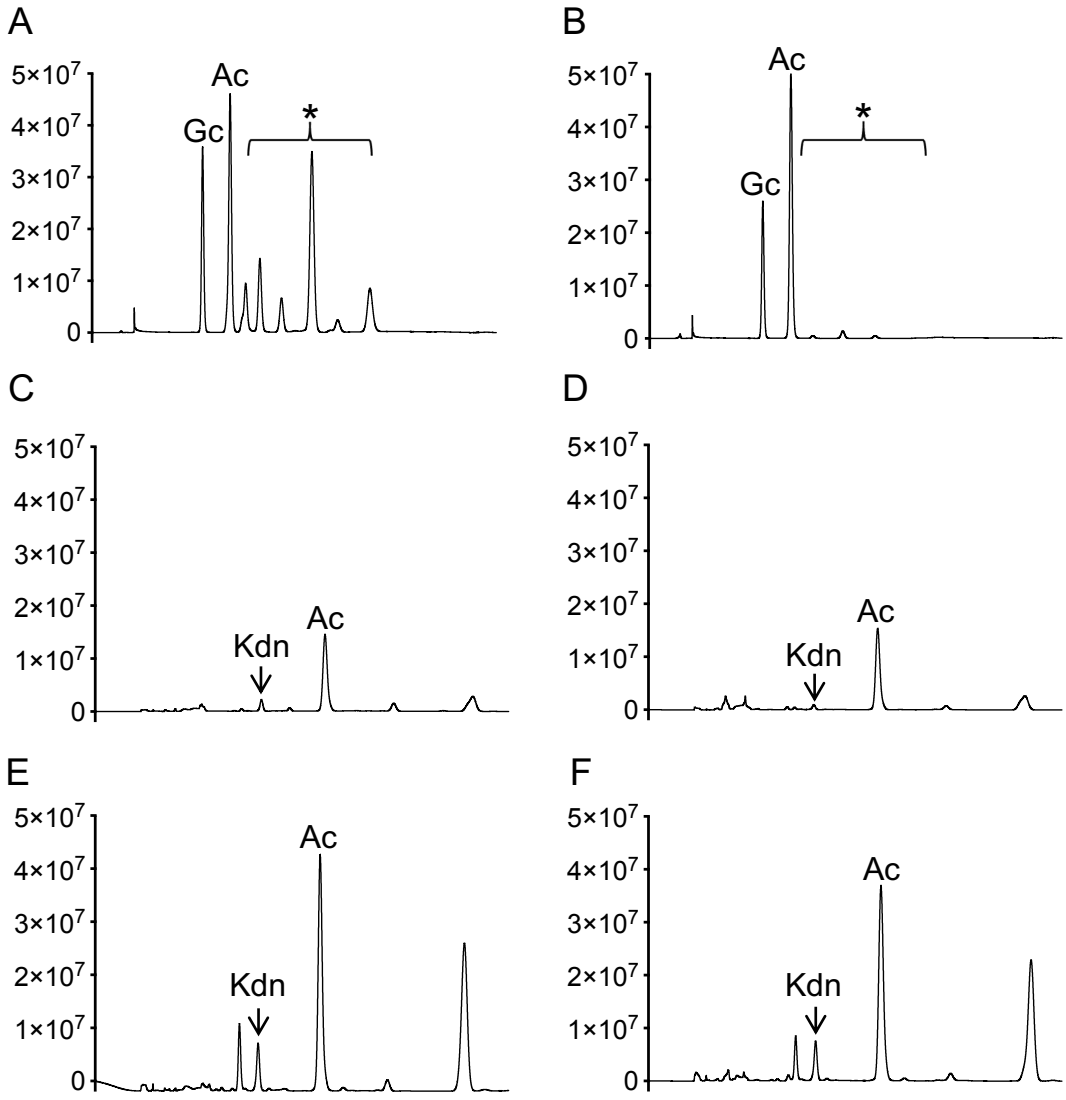

Supplemental Figure 1. HPLC analyses for free and CMP-sialic acid via de *O*-acetylation. (A) Bovine submaxillary mucin (BSM) was used as a standard for O-acetyl groups of sialic acids (Sias) and (B) the de-O-acetylation treatment. O-acetyl groups and solubilizing groups such as Neu5Gc7Ac, Neu5,7Ac2 (*) can be removed with NaOH treatment at 37˚C for 30 min. Control (C, D) and ESRD (E, F) serum samples did not show any significant peak shift (0-50 min in HPLC run) after NaOH treatment (D and F), suggesting that there was no O-acetyl form accumulation. Kdn, Neu5Ac (Ac), Neu5Gc (Gc) were annotated. Y-axis showed peak counts in HPLC run.

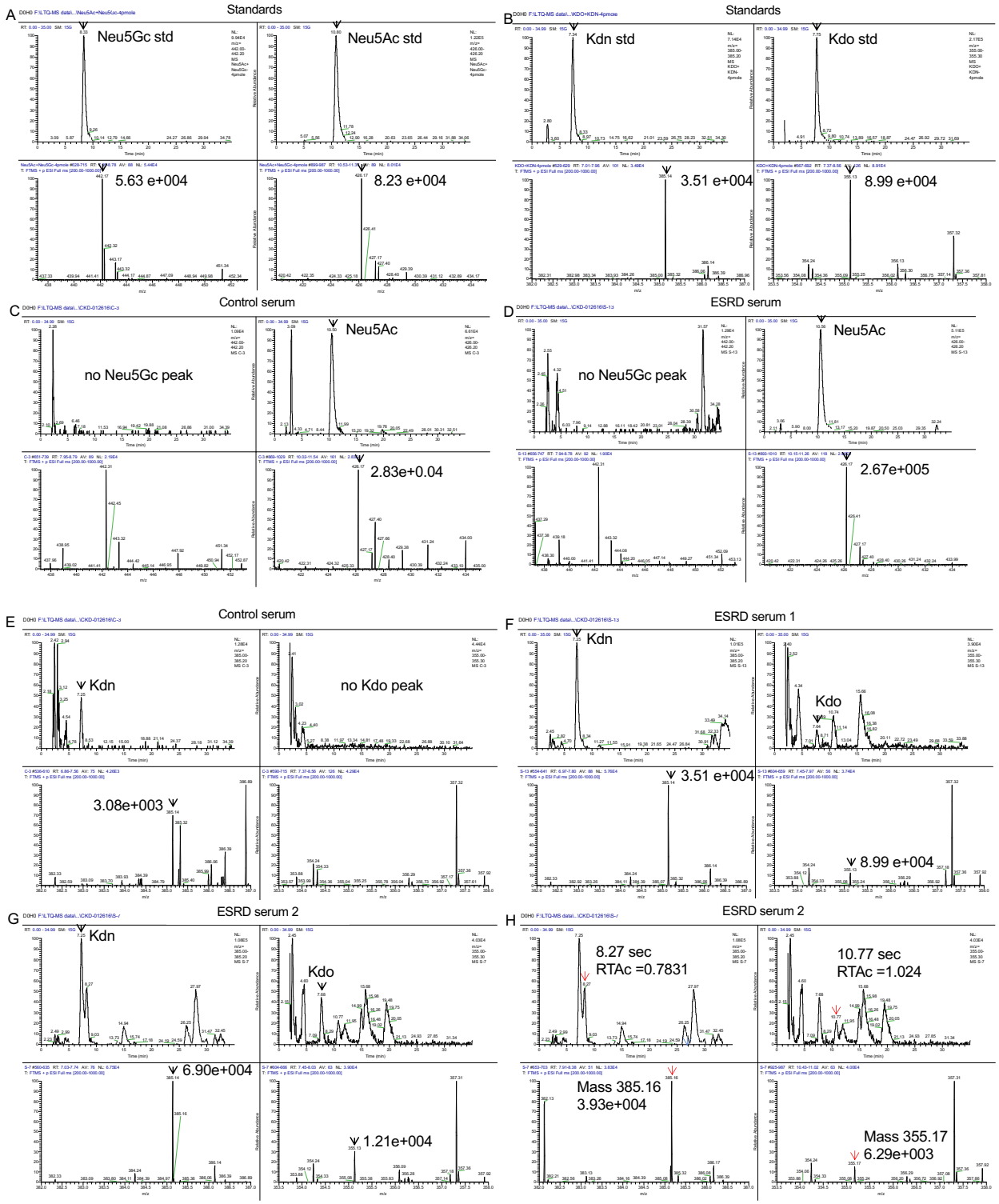

Supplemental Figure 2. LC/MS analyses for free α-ketoacids including sialic acids after DMB-tagging.

Peak analyses of standards (std) for (A) Neu5Gc and Neu5Ac, (B) Kdn and Kdo in LC-MS. Neu5Gc and Neu5Ac peaks in (C) control and, (D) end-stage of renal disease (ESRD) patient

serum. Kdn and Kdo peaks in (E) control and, (F), (G) ESRD. (H) Examples of unknown peaks that were found or significantly accumulated only in ESRD (red arrows). The same data are presented for (G) and (H) with different regions highlighted.

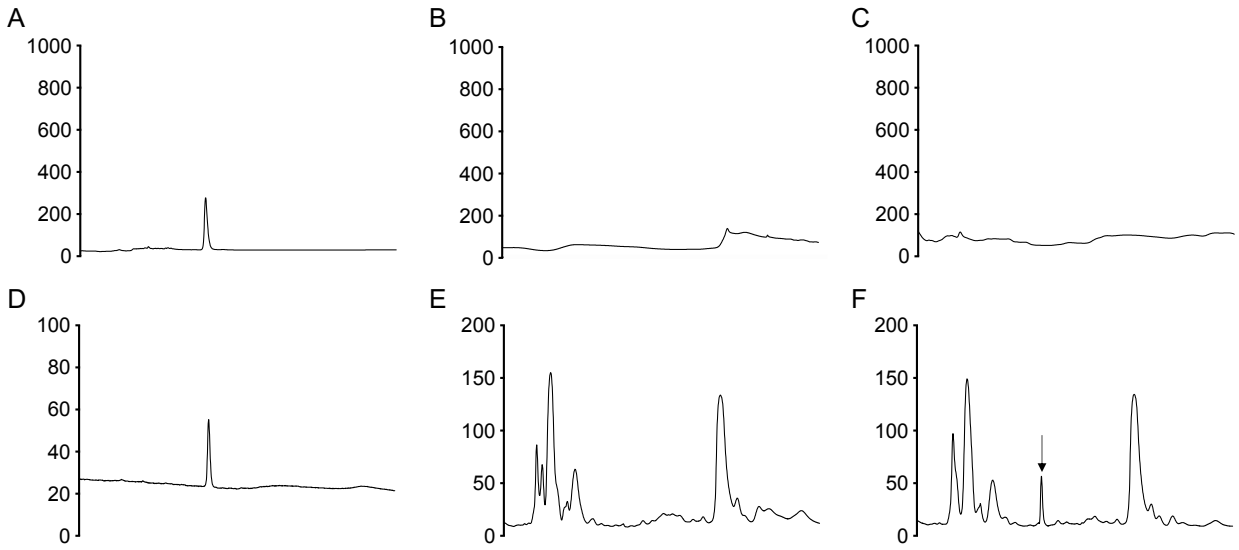

Supplemental Figure 3. HPAEC-PAD Analyses for Mannose-6P.

HPAEC-PAD peaks for (A) 0.2 μg (0.8 nmol) Man-6P standard for serum analysis; (B) without and (C) with external 0.2 μg Man-6P adding to the serum sample 1 hour after mannose ingestion when the serum mannose peak comes (Figure 3A). (D) Peaks for 0.2 μg Man-6P standard for urine analysis (E) without and (F) with external 0.2 μg Man-6P addition to the urine collected 4 hours after mannose ingestion when urine mannose peak comes. Man-6P is detected only in the spiked urine sample (arrow) (F), suggesting that Man-6P could not exist in human serum and urine, as well. Y-axis showed peak counts in HPAEC-PAD run.

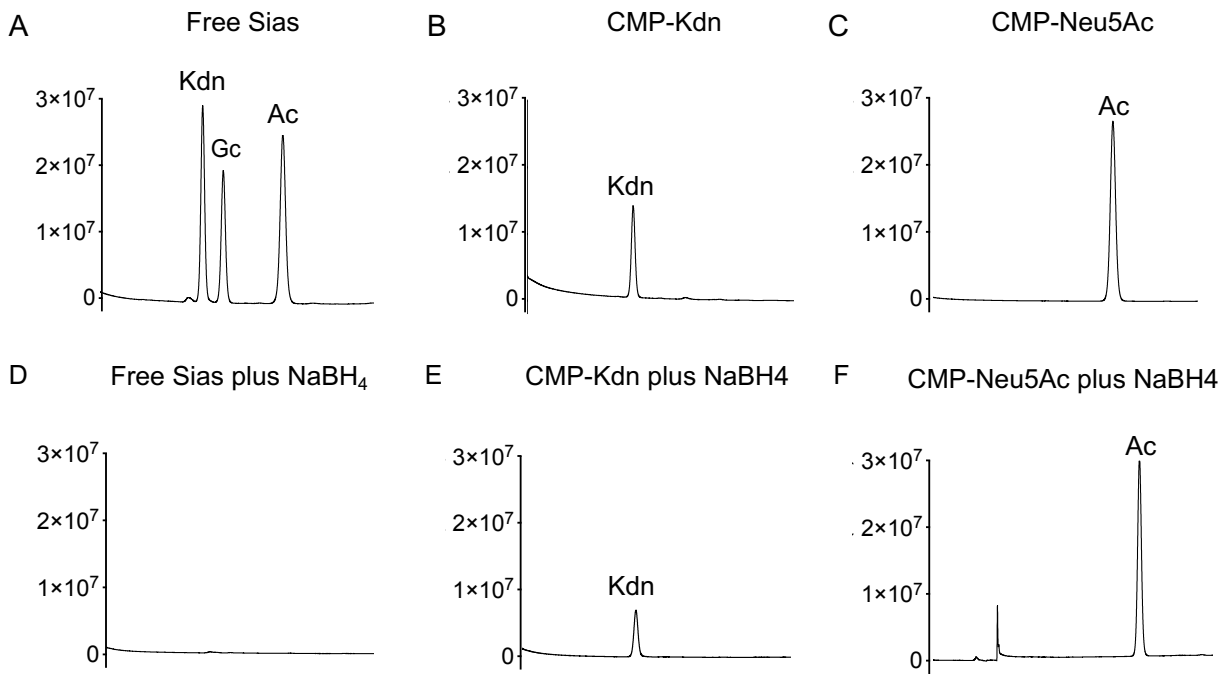

Supplemental Figure 4. DMB-HPLC analyses for free and CMP-activated form of sialic acids.

DMB-HPLC peaks for (A) free Sia 100 pmoles standards (Kdn, Neu5Gc (Gc) and Neu5Ac (Ac)); (B) CMP-Kdn; (C) CMP-Neu5Ac. (D) Free form of Kdn, Neu5Gc and Neu5Ac are sensitive to $NaBH_4$ treatment, but (E) CMP-Kdn and (F) CMP-Neu5Ac are resistant to $NaBH_4$.

Y-axis showed peak counts in HPLC run.

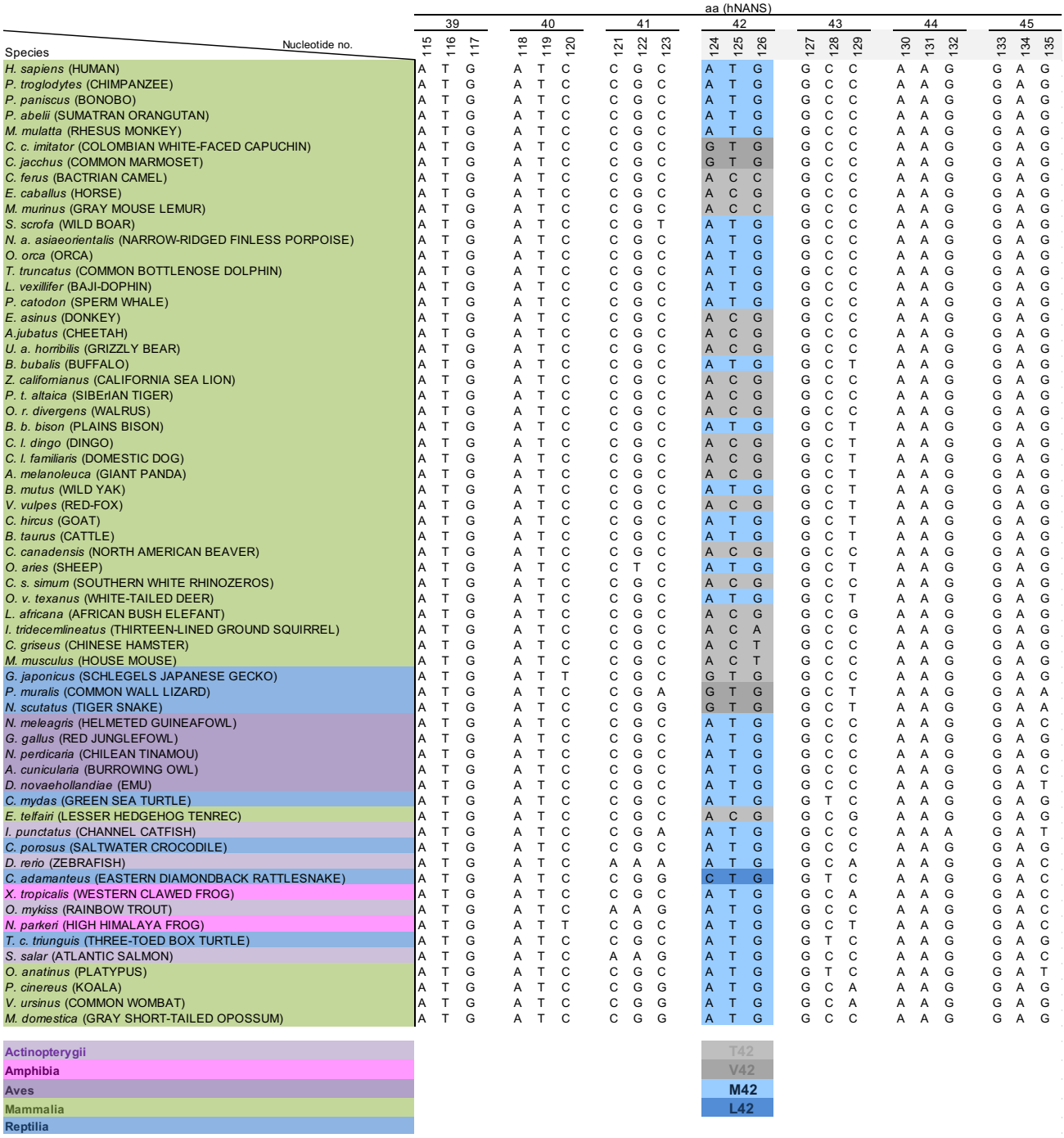

Supplemental Figure 5. Part of a multiple alignment of NANS nucleotide sequences

Codons specifying Methionine (M) and Leucine (L) at position 42 in human NANS (giving rise to NANS with Kdn synthase activity), are shaded in light and dark blue, respectively, while Threonine (T) and Valine (V) are shaded in light and dark grey. Species are shaded according to

classes: Actinopterygii (light purple), Amphibia (pink), Aves (dark purple) Mammalia (green), Reptilia (blue).

Supplemental Table 1. Standards used for Mass Spectrometry Analysis.

α-ketoacids	Abbreviation	Mass	Source
2-keto-3-deoxy-D-glycero-D-galacto-nononic acid	Kdn	385.14	Commercial
3-deoxy-D-manno-oct-2-ulosonic acid	Kdo	355.13	Commercial
N-glycolylneuraminic acid	Neu5Gc	442.16	Commercial
5,7-diamino-3,5,7, 9-tetradeoxy-D-glycero-D-galacto-non-2-ulosonic (legionaminic) acid	Leg	473	Commercial
7-O-acetyl-N-glycolylneuraminic acid	Neu5Gc7Ac	484.17	*BSM
N-acetylneuraminic acid	Neu5Ac	426.17	Commercial
8-O-acetyl-N-glyconeuraminic acid	Neu5Gc8Ac	484.17	BSM
5,7- diamino-3,5,7,9-tetradeoxy-L-glycero-L-manno-non-2-ulosonic (pseudaminic) acid	Pse	451	Commercial
7-O-acetyl-N-acetylneuraminic acid	Neu5,7Ac2	468.18	BSM
9-O-acetyl-N-glyconeuraminic acid	Neu5Gc9Ac	484.17	BSM
8-O-acetyl-N-acetylneuraminic acid	Neu5,8Ac2	468.18	BSM
9-O-acetyl-N-acetylneuraminic acid	Neu5,9Ac2	468.18	BSM
8,9-di-O-acetyl-N-acetylneuraminic acid	Neu5,8,9Ac3	510	BSM
7,9-di-O-acetyl-N-acetylneuraminic acid	Neu5,7,9Ac3	510	BSM

Each standard for α-ketoacids including sialic acids is available in commercial inventories including *bovine submaxillary mucin (BSM).

Kdn relative to Neu5Ac increased in various mammalian cells after mannose feeding.

Supplemental Table 2. Kdn relative to Neu5Ac in cytosol.

Cell line	Mannose concentration					
	0 mM	1 mM	3 mM	5 mM	10 mM	15 mM
HEK293A	0.24	0.27	0.31	0.31	0.38	0.42
HUVEC	0.07	0.22	0.22	1.01	3.82	3.02
BJAB K88	1.47	2.19	3.66	4.87	8.84	14.23
BJAB K20	5.18	10.39	49.12	28.84	26.91	90.62

Supplemental Table 3. Kdn relative to Neu5Ac in growth media.

Cell line	Mannose concentration		
	0 mM	5 mM	15 mM
HEK293A	0.127	0.526	1.418
HUVEC	1.128	1.130	1.624
BJAB K88	0.121	0.125	0.239
BJAB K20	0.149	0.453	1.780
PMI WT	0.098	0.416	0.604
PMI KO[#]	0.527	1.502	1.181
HK2	0.815	3.386	5.085

[#]The corresponding amounts of mannose for PMI KO cells were 25 μM, 250 μM and 1 mM.

Supplemental Table 4. *Total conjugated Kdn relative to Neu5Ac in total cell lysate with NaOH and $NaBH_4$.

Cell line	Mannose concentration		
	0 mM	5 mM	15 mM
HEK293A	0.000	0.000	0.000
HUVEC	0.001	0.002	0.003
BJAB K88	0.002	0.011	0.024
BJAB K20	0.013	0.054	0.165
PMI WT	0.000	0.003	0.004
PMI KO[#]	0.003	0.004	0.003

*Free sialic acids (Sias) and CMP-Sias were destroyed by $NaBH_4$ treatment.
It showed total cell conjugated form of Sias.
[#]The corresponding amounts of mannose for PMI KO cells were 25 μM, 250 μM and 1 mM.

Supplemental Table 5. Kdn relative to Neu5Ac in membrane fraction.

Cell line	Mannose concentration	
	0 mM	15 mM
HEK293A	0	0.0020
BJAB K88	0	0.064
BJAB K20	0.0042	0.11
PMI WT	0	0.0014
PMI KO[#]	0.012	0.0005
HK2	0	0.0035

[#]The corresponding amounts of mannose for PMI KO cells were 25 μM and 1 mM.

Supplemental Table 6. Kdn relative to Neu5Ac in membrane fraction of HEK293A with fish *Cmas* transfection.

vector	Mannose concentration	
	0 mM	15 mM
non-transfected	0	0.0014
empty vector	0	0.0019
*Cmas1	0.0043	0.0163
*Cmas2	0.0076	0.0323

*Two types of zebrafish CMP-sialic acid synthetases (Cmas) with differential substrate affinity were transiently expressed in HEK293A cells, and non-transfected and empty vector transfected cells were set as controls. Cells were harvested 36 hours post mannose feeding (0 or 15 mM) and membrane fractions were prepared to analyze glycosidically-conjugated form of sialic acids by DMB-HPLC analysis (Kdn relative to Neu5Ac).

Supplemental Table 7. Identity and homology of human and other vertebrate NANS proteins.

Species	Accession number (Protein)	Identity	Homology	Class
Acinonyx jubatus	XP_014934957.1	96%	98%	Mammalia
Ailuropoda melanoleuca	XP_002914976.1	96%	98%	Mammalia
Athene cunicularia	XP_026721911.1	84%	92%	Aves
Bison bison bison	XP_010845354.1	97%	99%	Mammalia
Bos mutus	XP_005906043.1	97%	99%	Mammalia
Bos taurus	NP_001039947.1	97%	99%	Mammalia
Bubalus bubalis	XP_006063515.1	97%	99%	Mammalia
Callithrix jacchus	XP_008998209.1	98%	99%	Mammalia
Camelus ferus	XP_006187837.1	97%	98%	Mammalia
Canis lupus dingo	XP_025287783.1	96%	98%	Mammalia
Canis lupus familiaris	XP_538746.2	96%	98%	Mammalia
Capra hircus	XP_005683962.2	97%	99%	Mammalia
Castor canadensis	XP_020036388.1	97%	98%	Mammalia
Cebus capucinus imitator	XP_017383327.1	98%	99%	Mammalia
Ceratotherium simum simum	XP_004423294.1	96%	98%	Mammalia
Chelonia mydas	XP_007066359.1	85%	93%	Reptilia
Cricetulus griseus	XP_003500141.1	95%	98%	Mammalia
Crocodylus porosu	XP_019410688.1	88%	93%	Reptilia
Crotalus adamanteus	AFJ51454.1	84%	94%	Reptilia
Danio rerio	NP_996660.1	79%	92%	Actinopterygii
Dromaius novaehollandiae	XP_025955160.1	85%	94%	Aves
Echinops telfairi	XP_004711046.1	92%	97%	Mammalia
Equus asinus	XP_014715223.1	96%	98%	Mammalia
Equus caballus	XP_023485493.1	96%	98%	Mammalia
Gallus gallus	NP_001007976.1	87%	94%	Aves
Gekko japonicus	XP_015281630.1	84%	94%	Reptilia
Homo sapiens	NP_061819.2	100%	100%	Mammalia
Ictalurus punctatus	NP_001187692.1	78%	91%	Actinopterygii
Ictidomys tridecemlineatus	XP_005326366.1	96%	98%	Mammalia
Lipotes vexillifer	XP_007461720.1	97%	98%	Mammalia
Loxodonta africana	XP_003407624.1	95%	98%	Mammalia
Macaca mulatta	EHH23940.1	99%	99%	Mammalia

Microcebus murinus	XP_012624488.1	97%	99%	Mammalia
Monodelphis domestica	XP_001364128.1	87%	94%	Mammalia (Methateria)
Mus musculus	NP_444409.1	95%	97%	Mammalia
Nanorana parkeri	XP_018407945.1	76%	89%	Amphibia
Neophocaena asiaeorientalis asiaeorientalis	XP_024590225.1	97%	98%	Mammalia
Notechis scutatus	XP_026528761.1	84%	94%	Reptilia
Nothoprocta perdicaria	XP_025893877.1	84%	91%	Aves
Numida meleagris	XP_021236216.1	87%	94%	Aves
Odobenus rosmar divergens	XP_004392385.1	95%	98%	Mammalia
Odocoileus virginianus texanus	XP_020761234.1	96%	99%	Mammalia
Oncorhynchus mykiss	XP_021429201.1	79%	91%	Actinopterygii
Orcinus orca	XP_004271519.1	96%	98%	Mammalia
Ornithorhynchus anatinus	XP_001506765.1	89%	95%	Mammalia (Monotremata)
Ovis aries	XP_004005320.3	97%	99%	Mammalia
Pan paniscus	XP_008972309.1	99%	99%	Mammalia
Pan troglodytes	XP_024201562.1	100%	100%	Mammalia
Panthera tigris altaica	XP_007089351.1	96%	98%	Mammalia
Phascolarctos cinereus	XP_020860268.1	90%	94%	Mammalia (Methateria)
Physeter catodon	XP_023982297.1	97%	98%	Mammalia
Podarcis muralis	XP_028568080.1	85%	94%	Reptilia
Pongo abelii	XP_002820068.1	99%	99%	Mammalia
Salmo salar	ACI33492.1	79%	91%	Actinopterygii
Sus scrofa	NP_001172068.1	97%	99%	Mammalia
Terrapene carolina triunguis	XP_024062240.2	85%	93%	Reptilia
Tursiops truncatus	XP_004322851.1	97%	98%	Mammalia
Ursus arctos horribilis	XP_026361945.1	95%	98%	Mammalia
Vombatus ursinus	XP_027714871.1	89%	94%	Mammalia (Methateria)
Vulpes vulpes	XP_025868953.1	96%	98%	Mammalia
Xenopus tropicalis	XP_002935918.1	76%	90%	Amphibia
Zalophus californianus	XP_027470724.1	95%	98%	Mammalia

Identity (%) and homology (%) of vertebrate NANS protein sequences to H. sapiens NANS

NCBI Reference Sequence Numbers are given and species are shaded according to classes: Actinopterygii, Amphibia, Aves, Mammalia, Reptilia.

Supplementary Table 8. Eukaryotic NANS sequences

Species	Class	Order	Family	Accession number (Protein)	Accession number (mRNA)	Common name
Acinonyx jubatus	Mammalia	Carnivora	Felidae	XP_014934957.1	XM_015079471.2	Cheetah
Ailuropoda melanoleuca	Mammalia	Carnivora	Ursidae	XP_002914976.1	XM_002914930.3	Giant panda
Athene cunicularia	Aves	Strigiformes	Strigidae	XP_026721911.1	XM_026866110.1	Burrowing owl
Bison bison bison	Mammalia	Artiodactyla	Bovidae	XP_010845354.1	XM_010847052.1	Plains bison
Bos mutus	Mammalia	Artiodactyla	Bovidae	XP_005906043.1	XM_005905981.2	Wild yak
Bos taurus	Mammalia	Artiodactyla	Bovidae	NP_001039947.1	NM_001046482.1	Cattle
Bubalus bubalis	Mammalia	Artiodactyla	Bovidae	XP_006063515.1	XM_006063453.2	Buffalo
Callithrix jacchus	Mammalia	Primates	Callitrichidae	XP_008998209.1	XM_008999961.1	Common marmoset
Camelus ferus	Mammalia	Artiodactyla	Camelidae	XP_006187837.1	XM_006187775.2	Bactrian Camel
Canis lupus dingo	Mammalia	Carnivora	Canidae	XP_025287783.1	XM_025431998.1	Dingo
Canis lupus familiaris	Mammalia	Carnivora	Canidae	XP_538746.2	XM_538746.6	Domestic dog
Capra hircus	Mammalia	Artiodactyla	Bovidae	XP_005683962.2	XM_005683905.3	Goat
Castor canadensis	Mammalia	Rodentia	Castoridae	XP_020036388.1	XM_020180799.1	North American beaver
Cebus capucinus imitator	Mammalia	Primates	Cebidae	XP_017383327.1	XM_017527838.1	Colombian white-faced capuchin
Ceratotherium simum simum	Mammalia	Perissodactyla	Rhinocerotidae	XP_004423294.1	XM_004423237.2	Southern white rhinozeros
Chelonia mydas	Reptilia	Testudines	Cheloniidae	XP_007066359.1	XM_007066297.2	Green sea turtle
Cricetulus griseus	Mammalia	Rodentia	Cricetidae	XP_003500141.1	XM_027403145.1	Chinese hamster
Crocodylus porosus	Reptilia	Crocodilia	Crocodylidae	XP_019410688.1	XM_019555143.1	Saltwater crocodile
Crotalus adamanteus	Reptilia	Squamata	Viperidae	AFJ51454.1	JU175930.1	Eastern diamondback rattlesnake

Danio rerio	Actinopterygii	Cypriniformes	Cyprinidae	NP_996660.1	NM_206829.1	Zebrafish
Dromaius novohollandiae	Aves	Casuariiformes	Casuariidae	XP_025955160.1	XM_026099375.1	Emu
Echinops telfairi	Mammalia	Afrosoricida	Tenrecidae	XP_004711046.1	XM_004710989.1	Lesser hedgehog tenrec
Equus asinus	Mammalia	Perissodactyla	Equidae	XP_014715223.1	XM_014859737.1	Donkey
Equus caballus	Mammalia	Perissodactyla	Equidae	XP_023485493.1	XM_023629725.1	Horse
Gallus gallus	Aves	Galliformes	Phasianidae	NP_001007976.1	NM_001007975.1	Red junglefowl
Gekko japonicus	Reptilia	Squamata	Gekkonidae	XP_015281630.1	XM_015426144.	Schlegel's Japanese gecko
Homo sapiens	Mammalia	Primates	Hominidae	NP_061819.2	NM_018946.4	Human
Ictalurus punctatus	Actinopterygii	Siluriformes	Ictaluridae	NP_001187692.1	NM_001200763.2	Channel catfish
Ictidomys tridecemlineatus	Mammalia	Rodentia	Sciuridae	XP_005326366.1	XM_005326309.2	Thirteen-lined ground squirrel
Lipotes vexillifer	Mammalia	Artiodactyla	Lipotidae	XP_007461720.1	XM_007461658.1	Baji-dolphin
Loxodonta africana	Mammalia	Proboscidea	Elephantidae	XP_003407624.1 [	XM_003407576.2	African bush elephant
Macaca mulatta	Mammalia	Primates	Cercopithecidae	EHH23940.1	XM_015117229.2	Rhesus macaque
Microcebus murinus	Mammalia	Primates	Cheirogaleidae	XP_012624488.1	XM_012769034.1	Gray mouse lemur
Monodelphis domestica	Mammalia	Didelphimorphia	Didelphidae	XP_001364128.1	XM_001364091.4	Gray short-tailed opossum
Mus musculus	Mammalia	Rodentia	Muridae	NP_444409.1	NM_053179.3	House mouse
Nanorana parkeri	Amphibia	Anura	Dicroglossidae	XP_018407945.1	XM_018552443.1	High Himalaya frog
Neophocaena asiaeorientalis asiaeorientalis	Mammalia	Artiodactyla	Phocoenidae	XP_024590225.1	XM_024734457.	Narrow-ridged finless porpoise

Notechis scutatus	Reptilia	Squamata	Elapidae	XP_026528761.1	XM_026672976.1	Tiger snake
Nothoprocta perdicaria	Aves	Tinamiformes	Tinamidae	XP_025893877.1	XM_026038092.	Chilean tinamou
Numida melagris	Aves	Galliformes	Numididae	XP_021236216.1	XM_021380541.1	Helmeted guineafowl
Odobenus rosmarus divergens	Mammalia	Carnivora	Odobenidae	XP_004392385.1	XM_004392328.1	Walrus
Odocoileus virginianus texanus	Mammalia	Artiodactyla	Cervidae	XP_020761234.1	XM_020905575.1	White-tailed deer
Oncorhynchus mykiss	Actinopterygii	Salmoniformes	Salmonidae	XP_021429201.1	GBTD011617 35.1	Rainbow trout
Orcinus orca	Mammalia	Artiodactyla	Delphinidae	XP_004271519.1	XM_004271471.1	Orca
Ornithorhynchus anatinus	Mammalia	Monotremata	Ornithorhynchidae	XP_001506765	XM_001506715.5	Platypus
Ovis aries	Mammalia	Artiodactyla	Bovidae	XP_004005320.3	XM_004005271.3	Sheep
Pan paniscus	Mammalia	Primates	Hominidae	XP_008972309.1	XM_008974061.2	Bonobo
Pan troglodytes	Mammalia	Primates	Hominidae	XP_024201562.1	XM_024345794.1	Chimpanzee
Panthera tigris altaica	Mammalia	Carnivora	Felidae	XP_007089351.1	XM_007089289.2	Siberian tiger
Phasolarctos cinereus	Mammalia	Diprotodontia	Phascolarctidae	XP_020860268.1	XM_021004609.1	Koala
Physeter catodon	Mammalia	Artiodactyla	Physeteridae	XP_023982297.1	XM_024126529.2	Sperm whale
Podarcis muralis	Reptilia	Squamata	Lacertidae	XP_028568080.1	XM_028712247.1	Common wall lizard
Pongo abelii	Mammalia	Primates	Hominidae	XP_002820068.1	XM_002820022.4	Sumatran orangutan
Salmo salar	Actinopterygii	Salmoniformes	Salmonidae	ACI33492.1	BT045230.1	Atlantic salmon
Sus scrofa	Mammalia	Artiodactyla	Suidae	NP_001172068.1	NM_001185139.1	Wild boar
Terrapene carolina triunguis	Reptilia	Testudines	Emydidae	XP_024062240.2	XM_026646379.2	Three-toed box turtle
Tursiops truncatus	Mammalia	Artiodactyla	Delphinidae	XP_004322851.1	XM_004322803.2	Common bottlenose dolphin
Ursus arctos horribilis	Mammalia	Carnivora	Ursidae	XP_026361945.1	XM_026506160.1	Grizzly bear
Vulpes vulpes	Mammalia	Carnivora	Canidae	XP_025868953.1	XM_026013168.1	Red-fox
Vombatus ursinus	Mammalia	Diprotodontia	Vombatidae	XP_027714871.1	XM_027859070.1	Common wombat

Xenopus tropicalis	Amphibia	Anura	Pipidae	XP_002935918.1	XM_002935872.4	Western clawed frog
Zalophus californianus	Mammalia	Carnivora	Otariidae	XP_027470724.1	XM_027614923.	California sea lion

Vertebrate NANS sequences: Taxonomy, common names and accession numbers Taxonomy and common names of vertebrates included in phylogenetic analyses (Figure 5) are shown with species shaded according to classes: Actinopterygii (light purple), Amphibia (pink), Aves (dark purple) Mammalia (green), Reptilia (blue). NCBI Reference Sequence Numbers of NANS protein and mRNA sequences.